

RESEARCH ARTICLE

Strategies in regulating glioblastoma signaling pathways and anti-invasion therapy

Eunok Jung¹, Aurelio A. de los Reyes V^{1,2}, Kurt Jan A. Pumares², Yangjin Kim^{1,3*}

1 Department of Mathematics, Konkuk University, Seoul, Republic of Korea, **2** Institute of Mathematics, University of the Philippines Diliman, Quezon City, Philippines, **3** Mathematical Biosciences Institute and Department of Mathematics, Ohio State University, Columbus, Ohio, United States of America

* ahyouhappy@konkuk.ac.kr

Abstract

Glioblastoma multiforme is one of the most invasive type of glial tumors, which rapidly grows and commonly spreads into nearby brain tissue. It is a devastating brain cancer that often results in death within approximately 12 to 15 months after diagnosis. In this work, *optimal control theory* was applied to regulate intracellular signaling pathways of miR-451–AMPK–mTOR–cell cycle dynamics via glucose and drug intravenous administration infusions. Glucose level is controlled to activate miR-451 in the up-stream pathway of the model. A potential drug blocking the inhibitory pathway of mTOR by AMPK complex is incorporated to explore regulation of the down-stream pathway to the cell cycle. Both miR-451 and mTOR levels are up-regulated inducing cell proliferation and reducing invasion in the neighboring tissues. Concomitant and alternating glucose and drug infusions are explored under various circumstances to predict best clinical outcomes with least administration costs.

OPEN ACCESS

Citation: Jung E, de los Reyes V AA, Pumares KJA, Kim Y (2019) Strategies in regulating glioblastoma signaling pathways and anti-invasion therapy. PLoS ONE 14(4): e0215547. <https://doi.org/10.1371/journal.pone.0215547>

Editor: Joseph Najbauer, University of Pécs Medical School, HUNGARY

Received: December 14, 2018

Accepted: April 3, 2019

Published: April 22, 2019

Copyright: © 2019 Jung et al. This is an open access article distributed under the terms of the [Creative Commons Attribution License](https://creativecommons.org/licenses/by/4.0/), which permits unrestricted use, distribution, and reproduction in any medium, provided the original author and source are credited.

Data Availability Statement: All relevant data are within the manuscript and its Supporting Information files.

Funding: This work is resulted from the Konkuk University research support program (E.J.). This paper is also supported by the Korea National Research Foundation (NRF) grant funded by the Korean government (MEST): NRF-2017R1A2B2004651 (E.J.) and the Basic Science Research Program through National Research Foundation of Korea (NRF) funded by Ministry of Science, ICT and Future Planning:

Introduction

Glioblastoma multiforme (GBM) is the most common and the most aggressive type of brain cancer. The median length of survival time is approximately 12 to 15 months following diagnosis. GBM is characterized by anaplasia, nuclear atypia, cellular pleomorphism, mitotic activity, and more importantly, alternating phases of rapid proliferation and aggressive invasion into the surrounding brain tissue. This leads to an inevitably critical recurrence even after the surgical resection of the main tumor mass [1, 2]. The mainstay of treatment for GBM is surgery, followed by radiotherapy and chemotherapy. Despite advances in these approaches, glioma cells can still invade the neighboring tissues beyond detection leading to tumor recurrence. High probability of main treatment failure also encourages researchers to investigate the use of innovative treatments when the first line of therapy has failed, in order to improve clinical outcomes [3].

In the tumor microenvironment (TME), glioma cells encounter many challenges including hypoxia, acidity, and limited nutrient availability. To maintain rapid growth, tumor cells need to adapt to these biochemical changes and modify their metabolic activity by increasing glycolysis even in the presence of oxygen. This process is called the *Warburg effect* which requires consuming considerable amounts of glucose [4]. The tricarboxylic acid cycle, or *Krebs cycle*, plays an important role in the breakdown of organic fuel molecules and the survival in non-

(2018R1A2B6007288) (Y.K.). This work was funded by the University of the Philippines System Enhanced Creative Work and Research Grant (ECWRG 2016-1-030). K.J.A.P. is supported by the University of the Philippines-Office of International Linkages-Continuous Operational and Outcomes-based Partnership for Excellence in Research and Academic Training Enhancement (UP-OIL-COOPERATE) grant and the Department of Science and Technology-Accelerated Science and Technology Human Resource Development Program-National Science Consortium (DOST-ASTHRDP-NSC) Scholarship.

Competing interests: The authors have declared that no competing interests exist.

hypoxic normal differentiated cells. These molecules include glucose, fatty acids, and some amino acids. While differentiated cells favor this type of metabolism, which is very efficient in terms of ATP production, tumor cells adopt the inefficient aerobic glycolysis producing relatively large amounts of waste product in the form of lactic acid [5]. This may provide cancer cells the advantage of not having to depend on oxygen as an energy source especially in a hostile tumor microenvironment, thus leading to longer survival [6]. Inhibition of glycolysis may also prevent drug resistance thus a better understanding of this metabolic pathway may lead to better treatment options and clinical outcomes [7]. Developing strategies of metabolic adaptation, angiogenesis, and migration is critical for cancer cells in order to survive metabolic stress and ensure enough nutrient supply as tumor mass accumulates where glucose supply may fluctuate due to heterogeneous biochemical and biophysical conditions [8]. Therefore, adequate cellular responses to glucose withdrawal are critical for cancer cell survival. Cancer cells then activate the 5'-adenosine monophosphate activated protein kinase (AMPK) pathway under metabolic stress. It is the master cellular sensor of energy availability which enhances glucose uptake and conserve energy, thus avoiding cell death [9]. MicroRNAs, also abbreviated as miRNA, are approximately 22 nucleotide single-stranded non-coding ribonucleic acids (RNAs) that are known to regulate gene expression [10]. Dysregulation of microRNA expression has been linked to oncogenic and tumor suppressor activities in several types of cancer, including GBM [11, 12], where altered miRNA expression contributes to tumorigenesis [13, 14].

Godlewski *et al.* [8] identified an interesting mechanism of glioma cell migration and proliferation wherein a particular microRNA, miR-451, and its counterpart, AMPK complex (CAB39/LKB1/STRAD/AMPK), determine whether the cell favors growth at the expense of invasion or conversely. Moreover, they also identified a potential feedback loop between LKB1 and miR-451 allowing for a sustained and robust response to glucose withdrawal [15]. It was found out that (i) under high (normal) glucose conditions, up-regulation of miR-451 leads to the down-regulation of AMPK complex, which then leads to elevated proliferation and decreased migration of glioma cells and (ii) glucose withdrawal induces down-regulation of miR-451 and up-regulation of AMPK, which promotes cell migration with reduced proliferation.

The mathematical models developed by Kim *et al.* [14, 16, 17] describe the effects of the miR-451-AMPK core control system on cell proliferation and migration in glioblastoma. It explains the response of miR-451 to high and low glucose levels as well as the mutual antagonism between miR-451 and AMPK complex concentrations. Kim *et al.* [18] then extended the model to include the dynamics of mammalian target of rapamycin (mTOR), which is a protein kinase that links with other proteins as well as to the cell cycle dynamics, to form the miR-451-AMPK-mTOR core control system. This mutual antagonism between miR-451 and AMPK, which was predicted in these mathematical models [14, 16–18], was confirmed by recent experiments. For example, Ansari *et al.* [19] recently found that (i) the miR-451 transcription in GBM cells is induced by unrestricted activity of its transcription factor OCT1 (official gene symbol POU2F1) in the presence of abundant glucose, resulting in AMPK inhibition through direct targeting of CAB39 in the LKB1 complex; and (ii) the miR-451 level is inhibited through the phosphorylation and inactivation of OCT1 at S335 by AMPK in response to glucose depletion-induced metabolic stress, leading to a reciprocal negative feedback loop between miR-451 and AMPK. In this case, suppression of miR-451 in turn leads to sustained AMPK activities and a robust response to glucose withdrawal in GBM cells. The multiscale mathematical models [14, 16–18] also predict the growth-invasion cycling patterns of glioma cells in response to fluctuating glucose uptake in the tumor microenvironment. The core control system predicts bistability and hysteresis bifurcation when delayed down-regulation of miR-451 activities along certain molecular pathways would induce glioma cells to stay longer in the proliferative phase despite relatively low glucose concentrations, making this mechanism a therapeutic target.

The cell cycle represents an integrated series of events that regulates complex processes including cell proliferation, cell division and DNA replication, regulated by a complex hierarchy of genetic and metabolic networks which involves several transition states of varied lengths and checkpoints [20]. The stages of the cell cycle are as follows: (i) synthesis phase (S), a period where DNA replication occurs; (ii) gap phase 2 (G2), during which proteins required for mitosis are produced; (iii) mitosis phase (M), a period where chromatin condensation, nuclear envelope breakdown (NEBD), chromatid separation, and cytokinesis happens; (iv) gap phase 1 (G1), in which genes necessary for DNA replication are activated and the protein agents of S phase progression are accumulated; and (v) resting phase (G0), a state in which cells can exit the cell cycle and enter a phase of quiescence or relative inactivity [21]. The progression of mammalian cell cycle is tightly regulated by coordinated activation of cyclin-dependent kinases (CDKs) family [22]. The CDKs are positively regulated by cyclins and negatively by CDK inhibitors (CKIs) such as the proteins p15, p16, p21 and p27. In cancer cells, cyclins are over-expressed while CKIs are under-expressed which results in the dysregulation of the cell cycle, and promoting uncontrolled cell growth [20]. Tyson and Novak [23, 24] identified that the transition between two stable steady states, G1 and S–G2–M cell-cycle phases, are described using the kinetic relations of the model that is controlled by changes in cell mass.

A standard GBM treatment is surgery followed by chemotherapy and radiotherapy. However, even under best circumstances, the mean survival of this disease is about a year. Poor outcomes of standard care treatments are due to the topographically diffuse nature of the disease [25]. By the time of diagnosis, typical GBM cells may have widely spread throughout the brain tissue [26–28], increasing the potential of recurrence. Thus, annihilation of distant tumor satellites is implausible despite surgically removing all the essential tumor seen on enhanced MRI scan [29]. Knowing the exact margins of a tumor mass in real patients is indeed a daunting task. In this study, it is assumed that a major tumour mass has been surgically removed and that the infiltrative tumor cells are near the surgical site. The objective is to prevent the glioma cells from further diffusing into the surrounding brain tissue. Localization approach will be utilized, that is, glioma cell invasion will be blocked keeping them in a proliferative phase while also attempting to limit excessive growth before a second surgery [17]. Our analytical tool is primarily based on the framework of *optimal control theory*, which has been successfully used to make informed decisions involving biological models such as optimal treatment strategies in human immunodeficiency virus (HIV) models [30–33], tuberculosis [34–36], and cardiopulmonary resuscitation (CPR) techniques [37, 38]. Optimal control theory is also applied to the miR-451–AMPK core control system to determine the intravenous glucose and/or drug infusion protocols with least possible cost under various circumstances in de los Reyes, *et al.* [39].

Recently, Kim *et al.* [40] developed an intracellular signaling pathway model that extends the miR-451–AMPK–mTOR core control system including the cell cycle dynamics. In this work, a potential control problem is formulated in order to maintain high levels of miR-451 and mTOR (low levels of AMPK) inducing cell proliferation prohibiting cell motility and invasion to the neighboring tissues. With glucose levels as a key regulator of miR-451 activity which also activates mTOR in the downstream signaling pathway, glucose intravenous infusion is considered to up-regulate miR-451 and mTOR concentrations above certain threshold values. In addition, a drug suppressing the inhibitory effect of mTOR by the AMPK complex is incorporated. This drug can be administered concomitantly or alternately with glucose as a secondary intravenous infusion. The controls are then given by dose rates of glucose and drug intravenous administrations regulating upstream and downstream signaling pathway, respectively. Solution of the optimal control problem aims to determine infusion protocols with minimal glucose and drug amount, and least administration costs. Hence, glucose and drug levels are regulated to prevent rapid tumour growth, hyperglycemia, and further drug complications.

The results propose plausible glucose and drug intravenous infusion controls which indicate the time of administration, frequency, number of administrations, and dosages of glucose and drug per infusion.

In the current study, we will first present the miR-451–AMPK–mTOR–cell cycle intracellular signalling pathway developed by Kim *et al.* [40]. A drug module is incorporated to up-regulate mTOR activities inducing cell proliferation. Then an optimal control problem is formulated with the goal of activating miR-451 and mTOR levels through glucose and drug intravenous infusions. Two different infusion protocols will be explored, namely, concomitant and alternating glucose and drug intravenous administrations. Optimal solutions for two strategies are presented and results on frequency, dosage per infusion, total glucose and drug amount, and relative cost incurred in the administrations are compared. The conclusion section discusses and summarizes the optimal control results, and provides outlook for future research directions.

Materials and methods

Intracellular signaling dynamics model

In this section, we present the basic components of intracellular signalling pathway of tumor cell containing the core control miR-451–AMPK–mTOR and cell cycle pathway developed in Kim *et al.* [40], incorporating a drug which blocks the inhibitory pathway of mTOR by AMPK complex. The core control model identifies a key mechanism which determines the molecular switches between the proliferative and migratory phases in response to fluctuating glucose and drug levels. The simplified signaling pathways consists of five key determinants of the intracellular structure, namely, glucose level G , miR-451 level M , AMPK complex activity A , mTOR concentration R , and drug level D . The intracellular cell cycle dynamics are developed by Tyson and Novak [23, 24] including only the essential interactions for its regulation and control. The model captures the kinetics of chemical processes within the cell such as production, destruction, and different molecule interactions. The transition between two main steady states, G1 and S–G2–M phases, of the cell cycle are described using the kinetic relations of the model that is controlled by changes in cell mass. Powathil *et al.* [41] modified the model by using equivalent mammalian proteins, namely the Cdk-cyclin B complex [$CycB$], the APC-Cdh1 complex [$Cdh1$], the active form of the p53cdc-APC complex [$p53cdc_A$], the total p53cdc-APC complex [$p53cdc_T$], the active form of Plk1 protein [$Plk1$] and the cell mass [$mass$]. Also included are the effects of the changes in oxygen dynamics at the macroscopic level through the activation and inactivation of HIF-1 α . This results in changes in cell cycle length. In addition, the cell cycle inhibitory effect of p21 or p27 genes of HIF-1 α is incorporated. Kim *et al.* [40] proposed to link both the miR-451–AMPK–mTOR control system and the cell cycle dynamics to provide a mechanism driving the cell cycle to undergo the *quiescent* stage G0-phase depending on the concentration level of mTOR. Fig 1A depicts the detailed schematic diagram of the intracellular signalling networks including miR-451, AMPK complex, mTOR, and key players in the cell cycle module ($CycB$, $Cdh1$, $p53cdc_T$, $p53cdc_A$, $Plk1$). Kinetic interpretation of arrows and hammerheads represent induction and inhibition in the signaling network, respectively. The dimensionless diagram of the core control miR-451, AMPK complex, and mTOR linking to the cell cycle is depicted in Fig 1B. It should be noted that u_G and u_D are the sources of glucose and drug with decay rates μ_G and μ_D , respectively, which can be controlled exogenously. S_1 and S_2 are signaling sources to AMPK complex and mTOR, respectively, while α , β and γ are inhibition strengths, and ϕ denotes decay.

It has been shown that high (normal) glucose concentration yields over expression of miR-451 levels (down-regulation of AMPK complex and up-regulation of mTOR) leading to elevated cell proliferation and reduced migration, while low glucose levels leads to down-

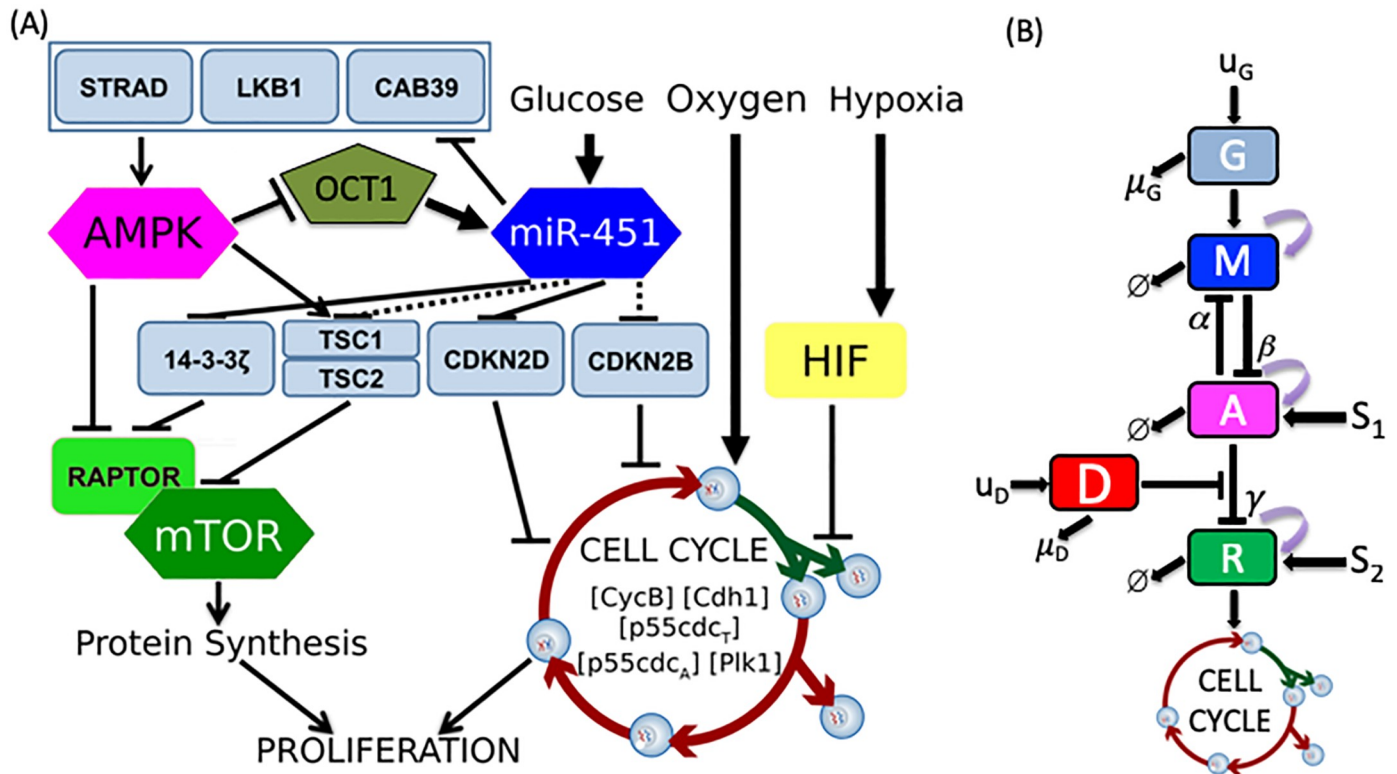


Fig 1. A model of the miR-451-AMPK-mTOR-cell cycle signaling pathway. (A) Detailed schematic diagram of cellular decision of proliferation and migration in glioblastoma [40]. (B) Block diagram of the theoretical model representing glucose (G) regulation on miR-451 (M), AMPK (A), mTOR (R) with the signaling pathway to the cell cycle dynamics and the drug (D) suppressing the inhibition of mTOR by AMPK.

<https://doi.org/10.1371/journal.pone.0215547.g001>

regulation of miR-451 activities (up-regulation of AMPK complex and down-regulation of mTOR) reducing cell proliferation and inducing migration into the surrounding brain tissue [8, 15, 18, 40]. The effect of various glucose levels in the regulation of the core control is depicted in Fig 2.

Kim *et al.* [14] developed a core control system of glioma cell migration and proliferation by using a regulatory network of key molecules (miR-451 (M), AMPK (A)) as follows:

$$\begin{aligned} \frac{dM}{dt} &= G + \frac{\ell_1 \ell_2^2}{\ell_2^2 + \alpha A^2} - M, \\ \frac{dA}{dt} &= \frac{1}{\epsilon_1} \left(S_1 + \frac{\ell_3 \ell_4^2}{\ell_4^2 + \beta M^2} - A \right). \end{aligned} \tag{1}$$

As observed in experiments [8, 15, 19], the regulatory system in Eq (1) includes a mutually antagonistic loop between miR-451 and AMPK complex in response to high and low glucose levels (G). This genetic toggle switch induces a monostable and bistable system, characterizing proliferation and critical cell infiltration of GBM cells in brain [14]. In the follow-up studies [14, 16–18] including mTOR (R) and cell cycle modules, this mutual antagonism and bistable system played a critical role in developing anti-invasion strategies. A mutually antagonistic feedback loop has been well-studied for its bistable properties by use of mathematical models ([42–45] and other references in [45]). For instance, in a study on a genetic toggle switch in *Escherichia coli* [42], a mutually inhibitory loop between repressor 1 and repressor 2 was

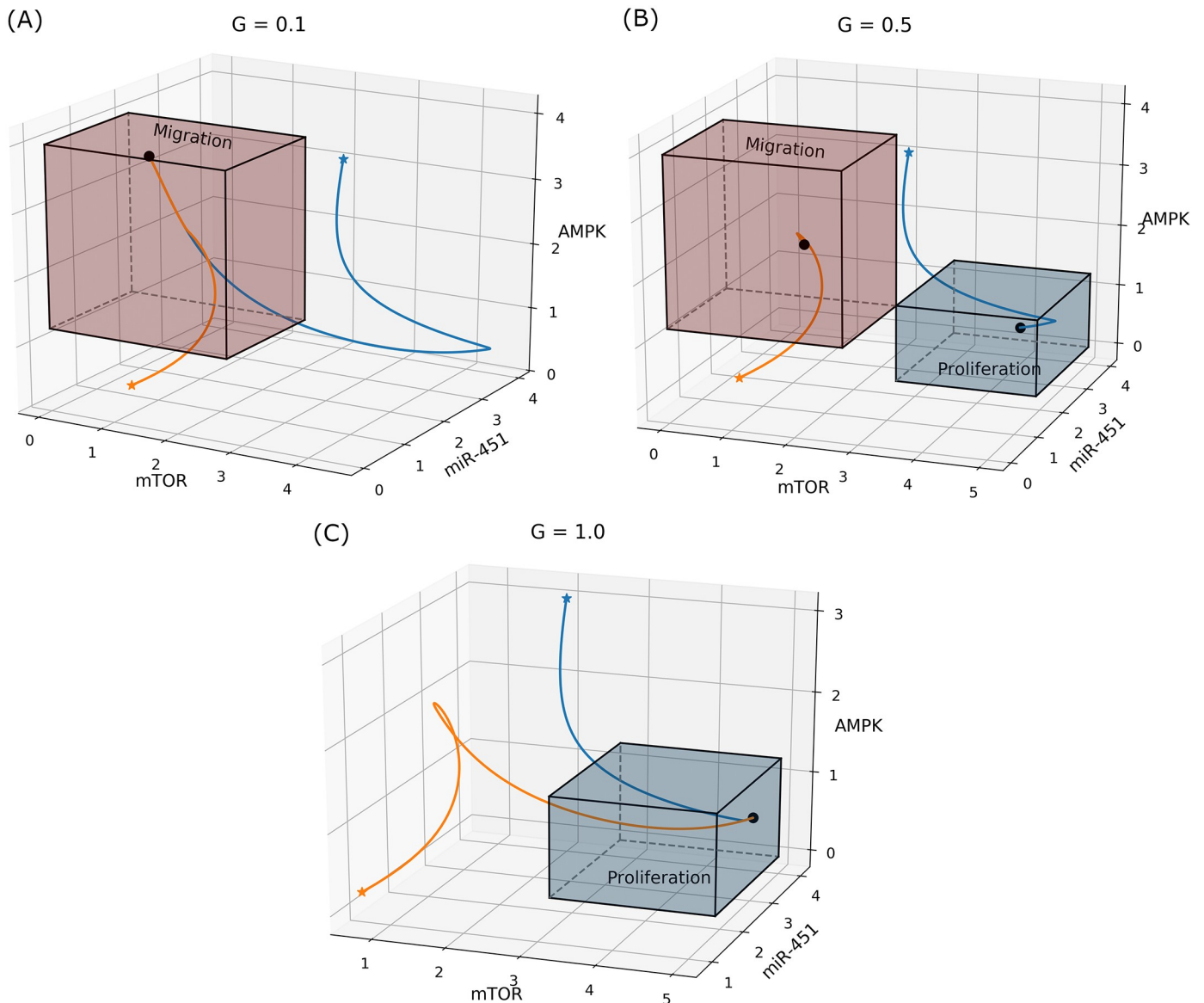


Fig 2. Effect of glucose on regulation of the core control system. Two trajectories of core control concentrations in miR-451–AMPK–mTOR space in response to (A) low ($G = 0.1$), (B) intermediate ($G = 0.5$), and (C) high ($G = 1.0$) glucose levels.

<https://doi.org/10.1371/journal.pone.0215547.g002>

shown to induce bistability in addition to monostable status. In particular, Lu *et al.* [45] in a theoretical study on miR-based regulation showed that the regulatory network including a mutual inhibition feedback circuit between the miR-34/SNAI1 and the miR-200/ZEB can induce a tristable circuit of epithelial-hybrid-mesenchymal fate differentiation. A detailed analysis on the self-activating, tristable state-inducing toggle switch or more general multistable genetic circuits can be found in [43, 44]. Other biological networks without mutual inhibition can also induce a bistable system. For instance, Aguda *et al.* [11] investigated the role of miRNAs in regulation of cell cycle and *cancer zone* by emerging bistable toggle switch in the feedback loops of miR-17-92, E2F, and Myc.

In this study, we consider a drug D suppressing the inhibitory effect of mTOR by AMPK complex where the inhibition strength is given by $\zeta(D) = e^{-D}$. When D is large, γe^{-D} is small

which makes dR/dt to be large. Thus, the presence of drug up-regulates mTOR activity that could eventually lead to cell proliferation. Fig 3 illustrates the mTOR bifurcation curve. Observe that increasing drug concentration shifts the hysteresis curve upwards keeping the same bistability window. Hence, with higher drug levels for the same glucose concentrations, mTOR is activated prompting elevated cell growth.

In the miR-451-AMPK-mTOR core control system developed by Kim and colleagues [14, 16–18, 40], the bistability regime of main variables emerges in response to glucose levels. As it was shown in [40], the existence and size of the bistability window ($|W^b|$) depend on other essential parameters and may disappear under perturbations of parameters. As it will be shown later (Figs 4 and 5), some of key parameters are sensitive in creation or destroying the bistability while other parameters are not. After achieving the equilibrium, continuation of the curve is computed by varying the glucose concentration G and bifurcation points are detected labeled LP and CP for limit and cusp points, respectively. Fig 6A illustrates the hysteresis diagram (G, R)–curves for different S_1 values. In order to obtain the cusp point (CP), fold continuation is computed starting at a limit point where two parameters G and S_1 are activated resulting to codim 2 bifurcations. Both parameters (G, S_1) are varied along the curve where each point is a limit point for the equilibrium curve at the corresponding value of S_1 . This is depicted in Fig 6B. The cusp point gives the threshold values $th_M, th_A,$ and th_R . A Matlab software `MatCont` was used for numerical continuation and bifurcation study of continuous and discrete dynamical systems [46].

The governing model equations for the dimensionless intracellular signaling dynamics are then described by the following ordinary differential equations

$$\begin{aligned}
 \frac{dG}{dt} &= u_1(t) - \mu_G G, \\
 \frac{dM}{dt} &= G + \frac{\ell_1 \ell_2^2}{\ell_2^2 + \alpha A^2} - M, \\
 \frac{dA}{dt} &= \frac{1}{\epsilon_1} \left(S_1 + \frac{\ell_3 \ell_4^2}{\ell_4^2 + \beta M^2} - A \right), \\
 \frac{dR}{dt} &= \frac{1}{\epsilon_2} \left(S_2 + \frac{\ell_5 \ell_6^2}{\ell_6^2 + \zeta(D)\gamma A^2} - R \right), \\
 \frac{dD}{dt} &= u_2(t) - \mu_D D, \\
 \frac{d[CycB]}{dt} &= k_1 - (k_2 + k_2'[Cdh1] + [p27/p21][HIF])[CycB], \\
 \frac{d[Cdh1]}{dt} &= \frac{(k_3 + k_3'[p55cdc_A])(1 - [Cdh1])}{J_3 + 1 - [Cdh1]} - \frac{k_4[mass_s][CycB][Cdh1]}{J_4 + [Cdh1]}, \\
 \frac{d[p55cdc_T]}{dt} &= k_5 + k_5' \frac{([CycB][mass_s])^n}{J_5^n + ([CycB][mass_s])^n} - k_6[p55cdc_T], \\
 \frac{d[p55cdc_A]}{dt} &= \frac{k_7[Plk1]([p55cdc_T] - [p55cdc_A])}{J_7 + [p55cdc_T] - [p55cdc_A]} - \frac{k_8[Mad][p55cdc_A]}{J_8 + [p55cdc_A]} - k_6[p55cdc_A], \\
 \frac{d[Plk1]}{dt} &= k_9[mass_s][CycB](1 - [Plk1]) - k_{10}[Plk1], \\
 \frac{d[mass]}{dt} &= \mu[mass] \left(1 - \frac{[mass]}{m^*} \right).
 \end{aligned}
 \tag{2}$$

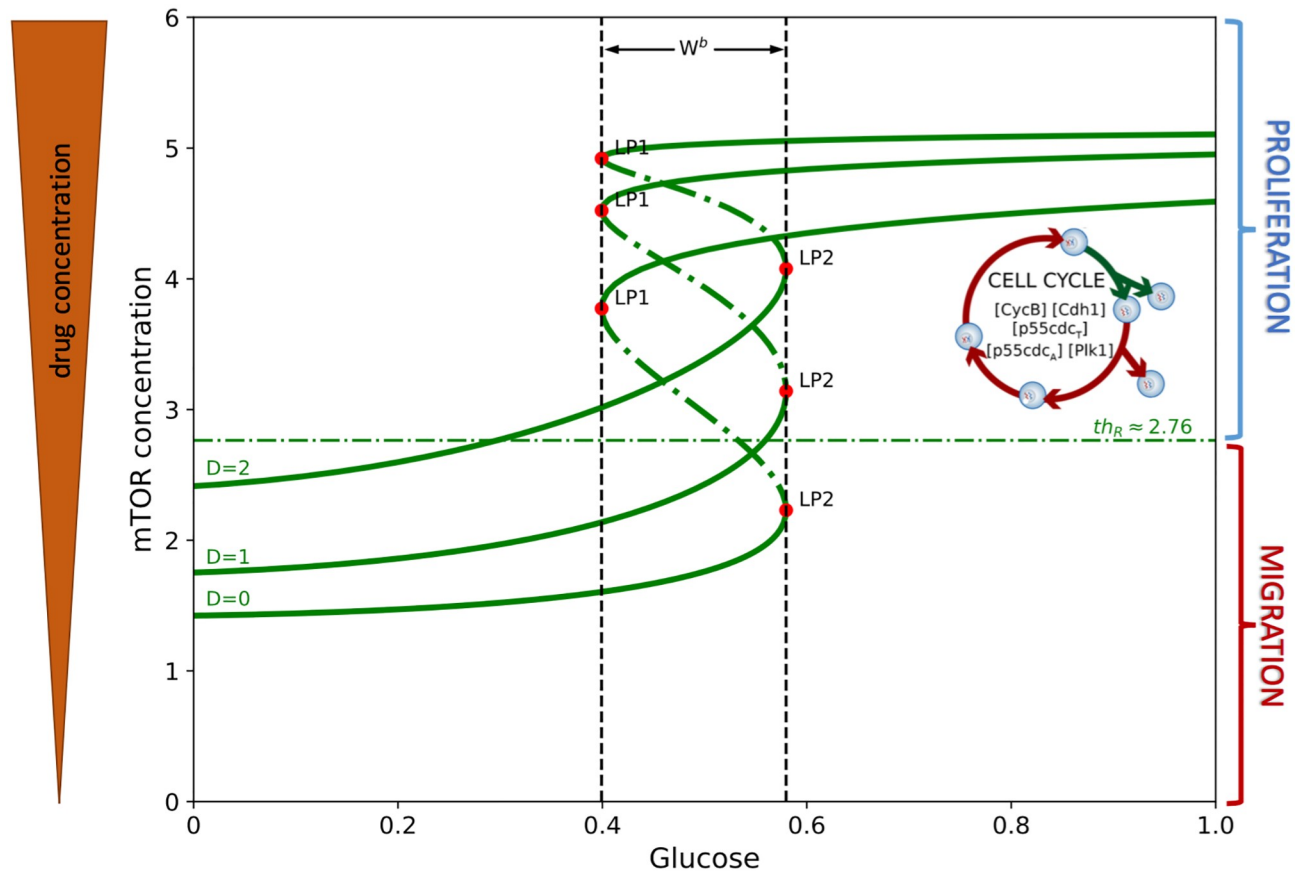


Fig 3. Bifurcation diagram of mTOR. Hysteresis diagram of mTOR concentration over the range of glucose levels and the corresponding effect of different drug concentrations on its dynamics.

<https://doi.org/10.1371/journal.pone.0215547.g003>

The cell cycle dynamics and the regulatory core control system are linked by a variable called *pseudo-mass* ($[mass_s]$) given by

$$[mass_s] = [mass] + \frac{\zeta_1 \left(\frac{1}{R}\right)^{n_1}}{K_m^{n_1} + \left(\frac{1}{R}\right)^{n_1}}. \tag{3}$$

The oxygen dynamics through HIF-1 α is described as

$$[HIF] = \frac{\zeta_2 \left(\frac{1}{K}\right)^{n_2}}{K_H^{n_2} + \left(\frac{1}{K}\right)^{n_2}}, \tag{4}$$

and the growth rate μ is expressed as

$$\mu = \mu^+ + \varepsilon \hat{\mu}, \tag{5}$$

where $\hat{\mu}$ is the probability density function with uniform distribution between -1 and 1 . This growth rate formulation introduces cell cycle heterogeneity of length between 20 and 30 hrs to

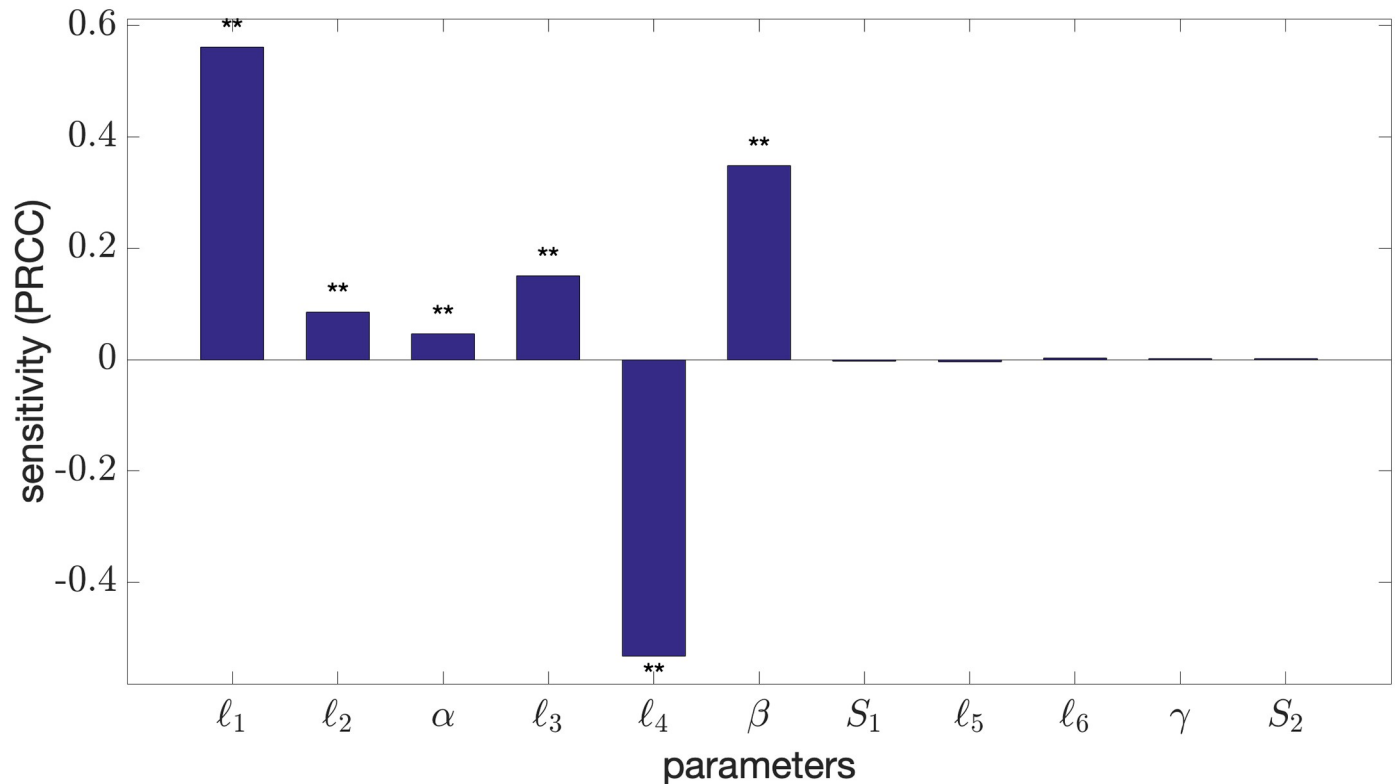


Fig 4. Sensitivity analysis on bistability of core control system. PRCC values of the core control model parameters influencing the bistability of the (G, R) hysteresis curve. The double asterisk (**) indicates a p-value of less than 0.01. The sample size carried out in the method is $N = 100,000$.

<https://doi.org/10.1371/journal.pone.0215547.g004>

account for the natural variability between cell growth rates and to have a non-synchronous population [41]. The model parameters in system (2) are listed in Tables 1 and 2.

In the current model formulation, mTOR (R) is activated/inactivated in the same way as miR-451 (M). In addition, R links the core control system and the cell cycle dynamics via the *pseudo-mass* ($[mass_s]$) which influences the cell mass $[mass]$ and the intracellular proteins (refer to Eq (3)). Therefore, when glucose supply is high, R is up-regulated (proliferative phase; up-regulated M , down-regulated A) and $[mass_s] \approx [mass]$ yielding a typical cell cycle (see Fig 7). On the other hand, when glucose supply is low, R is down-regulated (migratory phase; down-regulated M ; up-regulated A) and $[mass_s]$ exceeds $[mass]$ influencing the cells to enter into resting phase G0 [40].

Let us assume that glucose (G) and drug (D) can be regulated through intravenous infusions and can be periodically administered. For illustrative purposes, consider 3h infusions every 12h with maximum dosage of 1 unit, and refer this as *regular infusion*. We then have

$$u_j(t) = \begin{cases} 1 & \text{for } t \in [12n, 12n + 3], \quad n = 0, 1, 2, \dots \\ 0 & \text{otherwise.} \end{cases} \quad \text{for } j = G, D. \quad (6)$$

The intracellular dynamics under regular infusion can be seen in Fig 8. Since glucose and drug levels oscillate, it follows that M and R also periodically fluctuates around the threshold ($th_M \approx 1.87$, $th_R \approx 2.76$) as can be seen in Fig 8A. Note that when M and R crosses the threshold value from above, respectively, peak in pseudo-mass is generated. It can thus be inferred that these peaks indicate cell migration since M and R levels are below their respective threshold values.

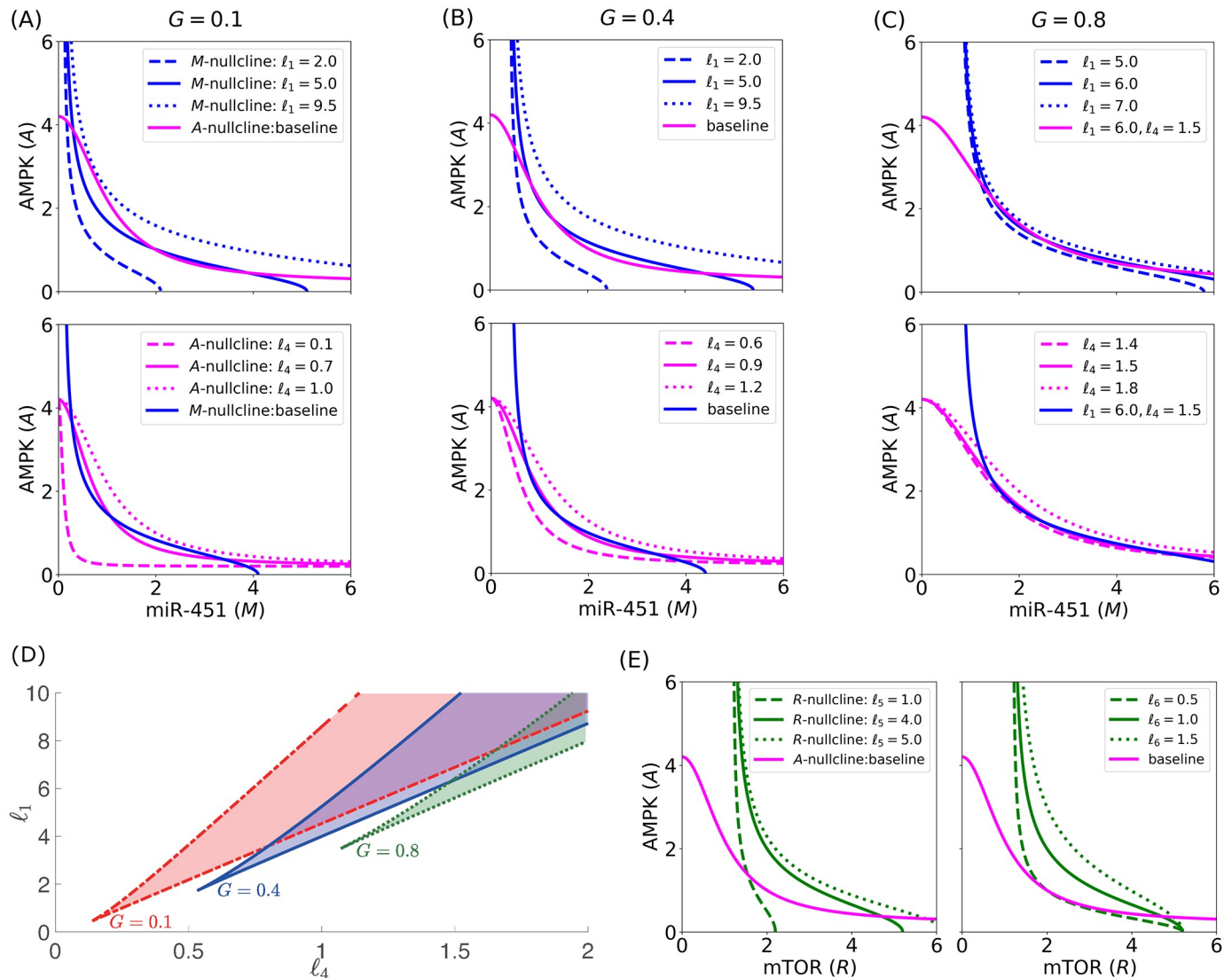


Fig 5. Effect of parameters l_1, l_4, l_5, l_6 on the core control nullclines and bistability. *M*- and *A*-nullclines for different l_1 and l_4 values for specific glucose levels: (A) $G = 0.1$, (B) $G = 0.4$, and (C) $G = 0.8$, showing instances of bistability and monostability. (D) Bifurcation curves for l_1 and l_4 and shaded region of bistability. (E) *R*- and *A*-nullclines for different l_5 and l_6 values showing monostability.

<https://doi.org/10.1371/journal.pone.0215547.g005>

As shown in Fig 8B, a trajectory of core control concentrations in mTOR-miR-451-AMPK space switches between proliferation and migration region. A closer look at the intracellular cell cycle proteins, mass, and mass_s dynamics are illustrated in Fig 8C. Note that regular infusion significantly perturb the cell cycle dynamics stimulating several cell divisions (see mass profiles) and cell migration (see mass_s). Indeed, fluctuating glucose levels in the microenvironment leads to the dichotomy of grow and go dynamics of glioblastoma cells yielding bigger tumor mass as reported in [14], even in the presence of (fluctuating) drug concentrations to keep the cells in proliferation phase.

Optimal control problem

In the current investigation, we aim to regulate the amount of glucose and drug infusions to up-regulate miR-451 and mTOR above its threshold values inducing cell proliferation

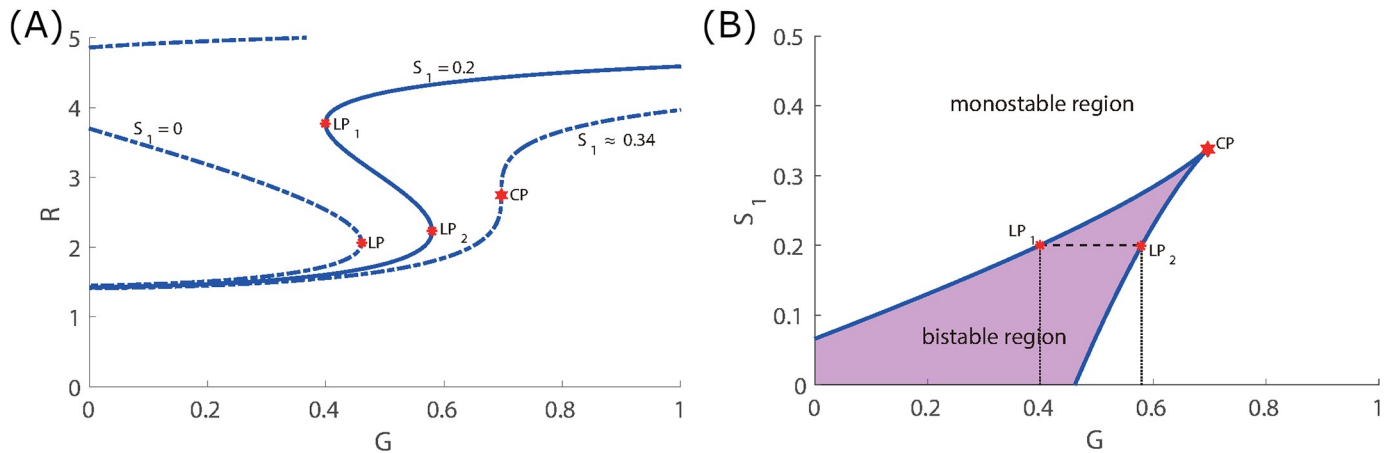


Fig 6. Codimension 2 bifurcation. (A) Hysteresis diagram of mTOR concentration over glucose level for three different values of $S_1 = 0, 0.2, 0.34$. (B) Codimension 2 bifurcation varying G and S_1 showing the equilibrium curves and cusp point (CP). Bistable and monostable regions are also depicted.

<https://doi.org/10.1371/journal.pone.0215547.g006>

avoiding migration to neighboring tissues. The modeling approach utilizes optimal control theory to identify infusion administration protocols. Let $u_G(t)$ and $u_D(t)$ be the controls of the system representing dose rates of glucose and drug intravenous administrations, respectively. Two different administration protocols are examined, namely, (1) *concomitant*, and (2) *alternating* glucose and drug infusions, with the following objective functionals

$$\begin{aligned}
 J_{\text{con}}(u_G(t), u_D(t)) &= \int_{t_0}^{t_1} \left(M(t) + R(t) - \left(\frac{B_1}{2} u_G(t)^2 + \frac{B_2}{2} u_D(t)^2 \right) \right) dt, \\
 J_{\text{alt}}(u_1(t), u_2(t)) &= \int_{t_0}^{t_1} \left(M(t) + R(t) - \frac{B_1}{2} u_G(t)^2 \right) dt \\
 &\quad + \int_{t_1}^{t_2} \left(R(t) - \frac{B_1}{2} u_D(t)^2 \right) dt,
 \end{aligned} \tag{7}$$

respectively. Here, $M(t)$ and $R(t)$ denote the level of miR-451 and mTOR concentrations, respectively. Parameters B_1 and B_2 are weight factors measuring the relative cost based on maximizing miR-451 $M(t)$ and mTOR $R(t)$, and administering glucose and drug intravenous infusions over a specified time interval, respectively. The control costs are modeled by the linear combination of quadratic terms $u_G^2(t)$ and $u_D^2(t)$. Our objective is to find optimal infusion regimen for glucose and drug administrations, denoted by $u_G^*(t)$ and $u_D^*(t)$, such that the objective functionals are satisfied, that is,

$$\begin{aligned}
 J_{\text{con}}(u_G^*(t), u_D^*(t)) &= \max_{\Omega_{\text{con}}} J_{\text{con}}(u_G(t), u_D(t)), \\
 J_{\text{alt}}(u_G^*(t), u_D^*(t)) &= \max_{\Omega_{\text{alt}}} J_{\text{alt}}(u_G(t), u_D(t)),
 \end{aligned} \tag{8}$$

where

$$\begin{aligned}
 \Omega_{\text{con}} &= \{u_G(t), u_D(t) \in \mathcal{L}(t_0, t_1) \mid 0 \leq u_G(t), u_D(t) \leq u_{\text{max}}, t \in [t_0, t_1]\}, \\
 \Omega_{\text{alt}} &= \{u_G(t) \in \mathcal{L}(t_0, t_1), u_D(t) \in \mathcal{L}(t_1, t_2) \mid \\
 &\quad 0 \leq u_G(t) \leq u_{\text{max}}, t \in [t_0, t_1], 0 \leq u_D(t) \leq u_{\text{max}}, t \in [t_1, t_2]\},
 \end{aligned} \tag{9}$$

Table 1. Parameters in the core control (miR-451-AMPK-mTOR) model.

Par	Description	Value	Ref
μ_G	glucose consumption rate	0.5	[17, 47]
ℓ_1	miR-451 autocatalytic production rate	4.0	[14, 17]
ℓ_2	Hill-type coefficient	1.0	[14, 17]
α	inhibition strength of miR-451 by AMPK complex	1.6	[14, 17]
th_M	threshold of miR-451 for invasion/growth switch	1.84	computed*
ℓ_3	AMPK autocatalytic production rate	4.0	[14, 17]
ℓ_4	Hill-type coefficient	1.0	[14, 17]
β	inhibition strength of AMPK complex by miR-451	1.0	[14, 17]
th_A	threshold of AMPK for invasion/growth switch	1.25	computed*
S_1	signaling source of AMPK	0.2	[14, 17]
ϵ_1	scaling factor (slow dynamics) of AMPK complex	0.02	[11, 14, 17, 48, 49]
ℓ_5	AMPK autocatalytic production rate	4.0	[14, 17]
ℓ_6	Hill-type coefficient	1.0	[14, 17]
γ	inhibition strength of AMPK complex by miR-451	1.0	[14, 17]
th_R	threshold of mTOR for invasion/growth switch	2.76	computed*
S_2	signaling source of mTOR	1.2	[14, 17]
ϵ_2	scaling factor (slow dynamics) of mTOR	0.02	[11, 14, 17, 48, 49]
μ_D	drug decay rate	1.316	[41, 50]

*The values are obtained using Matlab numerical bifurcation toolbox Matcont [46].

<https://doi.org/10.1371/journal.pone.0215547.t001>

The bounds for the controls represent the limits on dose rates for glucose and drug administrations. Assuming that miR-451, AMPK, and mTOR responses are regulated by glucose levels and influenced by drug levels, our control strategies deal with finding optimal control regimens for both glucose and drug intravenous infusions. We also note that the existence of optimal controls is guaranteed by standard results in control theory [51]. In this maximization problem, the necessary convexity of the integrand in the objective functional holds. Therefore, we can proceed with applying Pontryagin’s Maximum Principle [52]. An iterative method is used for solving the optimality system which is a two-point boundary value problem having initial conditions for the state variables and terminal conditions for the adjoints. Numerical simulations are obtained using a fourth-order iterative Runge-Kutta method. Given the initial conditions and guess for the controls, state equations are solved using the forward scheme while the corresponding adjoint equations are solved using the backward scheme with the transversality conditions. The controls are updated by using a convex combination of the previous controls and the value from the characterizations. This is commonly referred as the *Forward-Backward Sweep Method (FBSM)* which is shown to be convergent [53]. Further details on the optimal control under study can be found in the [S1 Appendix](#).

Results and discussion

Sensitivity analysis on bistability of the miR-451-AMPK-mTOR system

In Kim *et al.* [40] (see Fig S5 in Supplementary Appendix File in [40]), sensitivity analysis of the core control miR-451-AMPK-mTOR model (equations for M, A, R in Eq (2)) was performed in order to determine which parameters have the most/least influence on the reference output (main variables). All the core control parameters were considered to assess their corresponding influence on the miR-451, AMPK, and mTOR activity. It was inferred that miR-451

Table 2. Parameters in the cell cycle dynamics model.

Par	Description	Value	Ref
k_1	production rate of [CycB]	$0.12(h^{-1})$	[23, 24]
k_2	degradation rate of [CycB]	$0.12(h^{-1})$	[23, 24]
k_2'	degradation rate of [CycB] by [Cdh1]	$4.5(h^{-1})$	[23, 24]
[p27/p21]	inhibitory effect of p21 or p27 genes	1.05	[41]
K	oxygen concentration threshold	0.01	[41]
[CycB] _{th}	threshold for cell division	0.1	[23, 24]
k_3	activation rate of [Cdh1]	$3.0(h^{-1})$	[23, 24]
k_3'	activation rate of [Cdh1] by [p55cdc _A]	$30(h^{-1})$	[23, 24]
k_4	inactivation rate of [Cdh1] by [CycB]	$105(h^{-1})$	[23, 24]
J_3	Michaelis-Menten activation constant	0.04	[23, 24]
J_4	Michaelis-Menten inactivation constant	0.04	[23, 24]
k_5	production rate of [p55cdc _T]	$0.015(h^{-1})$	[23, 24]
k_5'	transcription rate of [p55cdc _T] by [CycB]	$0.6(h^{-1})$	[23, 24]
k_6	degradation rate of [p55cdc _T]	$0.3(h^{-1})$	[23, 24]
J_5	dissociation constant of [p55cdc _T]	0.3	[23, 24]
n	Hill coefficient	4.0	[23, 24]
k_7	activation rate of [p55cdc _A] by [Plk1]	$3.0(h^{-1})$	[23, 24]
k_8	inactivation rate of [p55cdc _A] by [Mad]	$1.5(h^{-1})$	[23, 24]
J_7	Michaelis-Menten activation constant	0.001	[23, 24]
J_8	Michaelis-Menten inactivation constant	0.001	[23, 24]
[Mad]	spindle checkpoint genes concentration	1.0	[23, 24]
k_9	activation rate of [Plk1] by [CycB]	$0.3(h^{-1})$	[23, 24]
k_{10}	degradation rate of [Plk1]	$0.06(h^{-1})$	[23, 24]
μ^+	specific growth rate	0.03	[23, 24]
m^*	maximum size to which a cell may grow	10	[23, 24]
ϵ	cell cycle heterogeneity growth rate parameter	0.006	[41]
ζ_1	Hill-type parameter in [mass _s]	2.5	[17]
n_1	Hill-type parameter in [mass _s]	10	[17]
K_m	Hill-type parameter in [mass _s]	0.5	[17]
ζ_2	Hill-type parameter in [HIF]	1.0	[41]
n_2	Hill-type parameter in [HIF]	10.0	[41]
K_H	Hill-type parameter in [HIF]	10.0	[41]
μ_D	Decay rate of drug	1.316	[41, 50]

<https://doi.org/10.1371/journal.pone.0215547.t002>

activity will be enhanced by increasing glucose signal (G) and autocatalytic production rates (ℓ_1, ℓ_2) of miR-451. These parameters were negatively correlated with AMPK activity due to the mutual antagonistic mechanism between miR-451 and AMPK complex. In addition, AMPK activity will be up-regulated by an increase in signaling source S_1 and autocatalytic rates (ℓ_3, ℓ_4) of the AMPK complex in the model. It has been also noted that increasing S_1 and the inhibition strength of mTOR by AMPK (γ) down-regulates mTOR level. In a similar fashion, S_2 is strongly positively correlated with mTOR levels but little correlated with $G, \ell_1, \ell_2, \ell_3, \ell_4, \alpha, \beta, \epsilon_1, \epsilon_2$ at time 100.

In this work sensitivity analysis is carried out to determine which model parameters have consequential effect in achieving or inhibiting bistability in the (G, R)–curve. As in [40], a method from [54] is adapted where a range for each parameter is selected and divided into N intervals of uniform length. For each parameter of interest, a partial rank

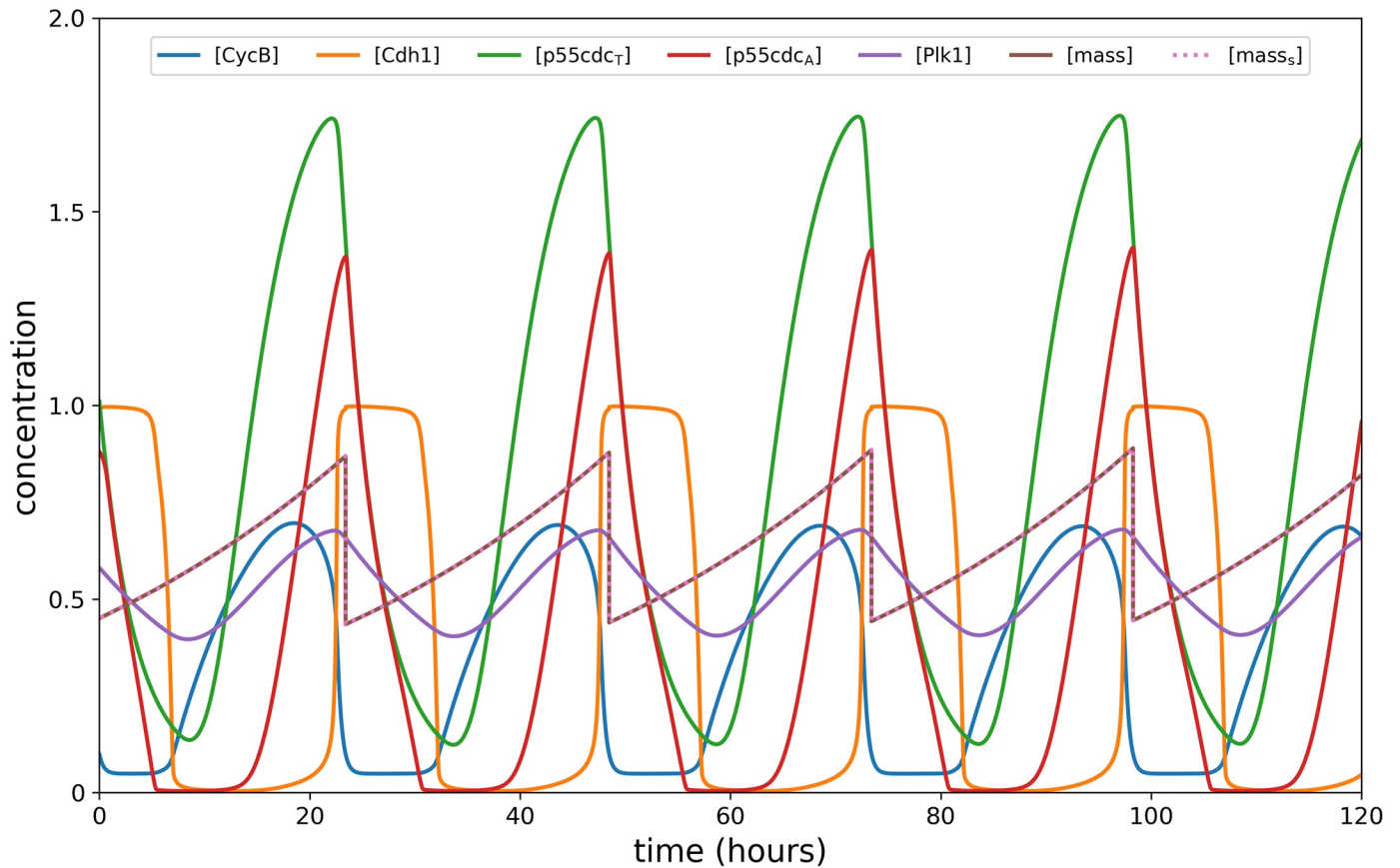


Fig 7. Typical cell cycle dynamics. Dynamics of intracellular proteins, mass, and mass_s of the cell cycle model in response to constant (intermediate) high glucose level.

<https://doi.org/10.1371/journal.pone.0215547.g007>

correlation coefficient (PRCC) value is computed. In order to obtain the PRCC values, *Latin Hypercube Sampling* (LHS), a stratified sampling without replacement technique, is chosen. The PRCC values range between -1 and 1 with the sign determining whether a change in the parameter value will promote (+) or suppress (−) bistability. The following algorithm is performed:

1. Assign a probability distribution $\mathcal{D}[\mu_{j,min}, \mu_{j,max}]$ to each parameter μ_j and let N be the number of samples to be selected. Divide the interval $[\mu_{j,min}, \mu_{j,max}]$ into N equiprobable subintervals, and draw an independent sample from each subinterval.
2. Assemble the LHS matrix L , wherein each row of L represents a unique combination of parameters sampled without replacement.
3. For each row of the LHS matrix L , solve for mTOR R in terms of glucose G and check for bistability window W^b . If bistability exists assign 1 to output variable W^b in matrix Y , else assign -1 .
4. Rank-transform the matrices L and Y to obtain L_R and Y_R . By rank-transform, we mean to replace the value by its rank when the data are sorted from lowest to highest, e.g. the smallest value is assigned a rank 1 . Tied values are assigned an average rank.

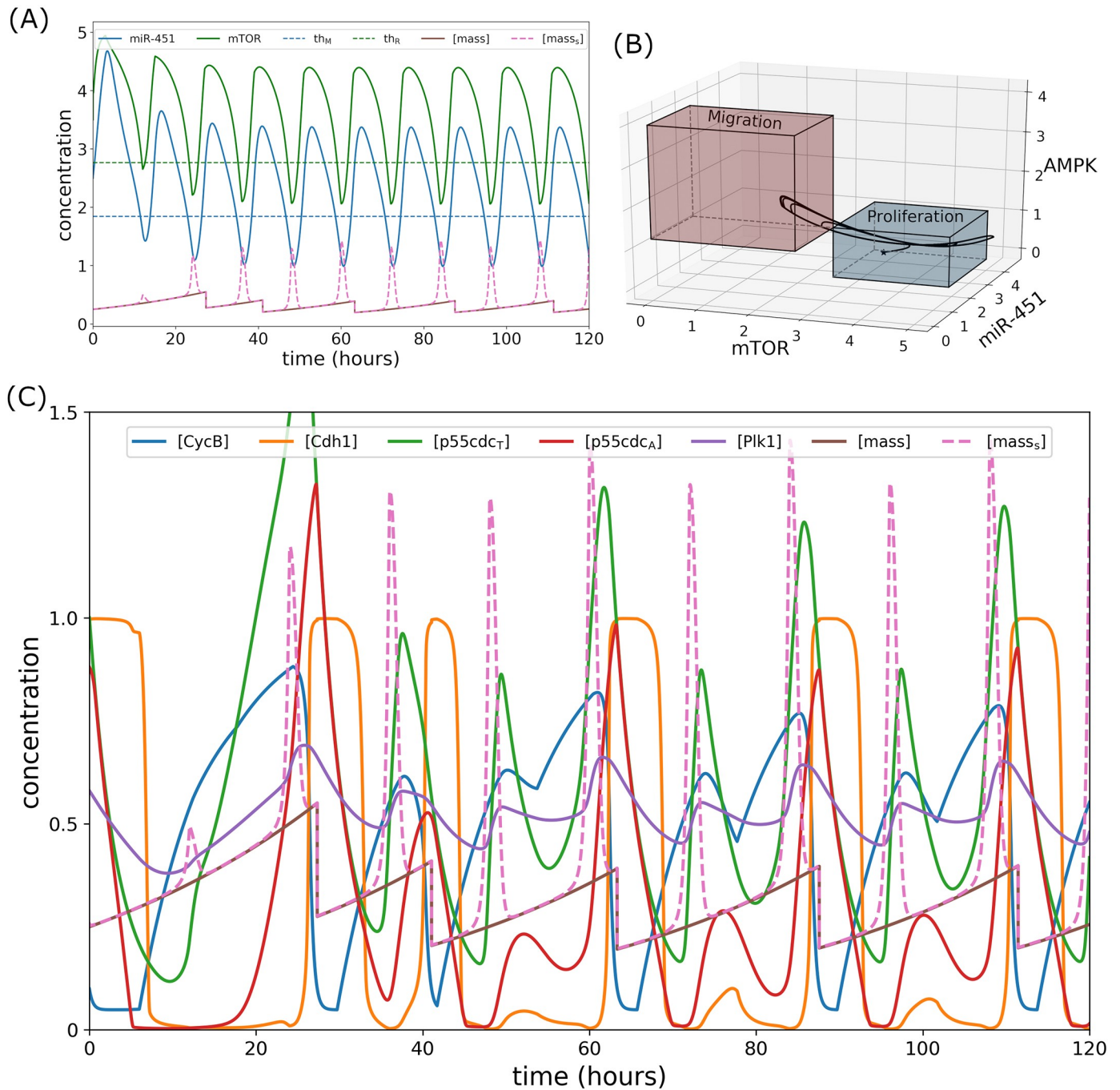


Fig 8. Intracellular dynamics under regular glucose and drug infusions. (A) Concentration profiles of miR-451 (M) and mTOR (R) fluctuating around the threshold values under regular infusions. Peaks in pseudo-mass are generated when M and R crosses th_M and th_R , respectively. (B) Trajectory of mTOR–miR-451–AMPK concentration profiles switching between proliferation and migration mode. (C) Dynamics of intracellular proteins, mass, and mass_s of the cell cycle model in response to regular glucose and drug infusions.

<https://doi.org/10.1371/journal.pone.0215547.g008>

- Fix a parameter μ_j , which is encoded in the j^{th} column in the matrix L_R . Form the following linear regression models using the data matrices L_R and Y_R for μ_j and y , respectively:

$$\hat{\mu}_j = c_0 + \sum_{p=1, p \neq j}^{n_p} c_p \mu_p, \tag{10}$$

$$\hat{y} = b_0 + \sum_{p=1, p \neq j}^{n_p} b_p \mu_p. \tag{11}$$

Compute $(\mu_j - \hat{\mu}_j)$ and $(y - \hat{y})$, the residuals in the input parameter and the output after removing the linear effects of the other input parameters.

- Obtain the PRCC of μ_j using

$$PRCC_{\mu_j, y} = \frac{\text{Cov}(\mu_j - \hat{\mu}_j, y - \hat{y})}{\sqrt{\text{Var}(\mu_j - \hat{\mu}_j)\text{Var}(y - \hat{y})}}. \tag{12}$$

- Repeat Steps 5 and 6 for the remaining parameters.

Fig 4 shows the sensitivity (PRCC value) of the model parameters in promoting (+) or destroying (−) bistability. It illustrates that a change in the miR-451 autocatalytic production rate (ℓ_1) or inhibition strength of AMPK complex by miR-451 (β) enhances bistability. On the contrary, the Hill-type coefficient ℓ_4 in the regulation of AMPK is responsible for losing bistability. It should be noted that due to the model’s structure, ℓ_1 up-regulates miR-451 which in turn increases mTOR and suppress AMPK activity. The parameter ℓ_4 promotes AMPK complex and down-regulates miR-451 and mTOR. However, other parameters $\ell_2, \alpha, \ell_3, S_1, \ell_5, \ell_6, \gamma, S_2$ are little sensitive in emergence or destruction of the bistability.

The bistability of miR-451–AMPK–mTOR core control system depends on the geometric structure of its nullclines. In particular, bistability arises when M - and A -nullclines (i.e., $\frac{dM}{dt} = 0$ and $\frac{dA}{dt} = 0$) intersect at three distinct points, producing one unstable and two stable steady states. The nullclines intersect three times due to their sigmoidicity influenced by catalytic rates ℓ_1 and ℓ_4 . These rates must be proportionate for a given glucose G level. Otherwise, the nullclines will intersect only once. This bistability condition has been shown for a genetic toggle switch in *E. coli* [42]. Fig 5A–5C depict the M - and A -nullclines under different G levels with various ℓ_1 and ℓ_4 values. The bifurcation curves for ℓ_1, ℓ_4 and region of bistability for specific G levels are depicted in Fig 5D. Under given circumstances, ℓ_1 and ℓ_4 showed significant sensitivities in the bistability of the system. On the contrary, both ℓ_5 and ℓ_6 affect the R -nullcline only. It is illustrated in Fig 5E that for several ℓ_5 and ℓ_6 values, R - and A -nullclines intersect at only one point, leading to a single steady state. In effect, M - and A -nullclines will also intersect once, producing monostability. Hence, ℓ_5 and ℓ_6 show insignificant consequence in achieving bistability (see Fig 4).

In the following numerical experiments, it is assumed that initially glioma cells are in growth phase (a probable occurrence of post primary tumour surgery) with $M > th_M, A < th_A$, and $R > th_R$. It is also considered that glucose and drug can be administered exogenously as intravenous infusions. Further, the weight parameters $B_1 = 1$ and $B_2 = 1$ are used as default values unless specified.

Concomitant infusion control

In this strategy, glucose and drug infusions are administered simultaneously, in particular, both controls $u_G(t)$ and $u_D(t)$ are infused at the same. Thus, this is referred to as *concomitant*

control. Here, it is assumed that the drug in consideration which blocks the inhibitory pathway of mTOR by AMPK complex had negligible side effects and had inconsequential chemical reactions with glucose. In order to determine an efficient strategy of concomitant infusion protocol, glucose and drug are administered concurrently at initial time $t = 0$ for 3 hours using the numerical scheme FBSM. Infusion spontaneously increases glucose and drug concentrations as depicted in Fig 9(A) and 9(B). Consequently, miR-451 and mTOR levels are up-regulated while AMPK complex is down-regulated as shown in Fig 9C. A closer look at the control curves shows that both $u_G(t)$ and $u_D(t)$ decrease from $0 < t_i < 3$ suggesting that both glucose and drug dose rates should be decreased from time t_i . This leads to the decrease of glucose and drug concentrations due to consumption and decay. Accordingly, miR-451 and mTOR levels decrease while AMPK complex increases. Before miR-451 crosses the threshold value th_M , FBSM is again applied for the next 3 hours. This suggests a time for the next concomitant administrations in which miR-451 profiles are monitored subsequently. The procedures in tracking miR-451 profiles and applying FBSM for 3 hours are repeated over a specified time duration. Thus, the number of concomitant administrations are determined. It is important to note that keeping miR-451 level above its threshold value consequently confine AMPK and mTOR levels, below and above its corresponding threshold values, respectively (see Fig 9C). Fig 10 depicts the intracellular dynamics under concomitant glucose and drug control. In Fig 10A, it can be observed that both miR-451 and mTOR levels are above their threshold values, and $[mass_s] \approx [mass]$. Under concomitant control, the trajectory of mTOR–miR-451–AMPK concentration profiles are restricted only in the proliferation region as shown in Fig 10B. The time courses of cell cycle variables under concomitant control is illustrated in Fig 10C. It can be seen that concomitant control induces fewer (only 3) mass divisions over 120h period as compared to regular infusions with 5 mass divisions, see Fig 8C. It should be noted as well that in concomitant control, mass concentration is increased before division.

Alternating infusion control

Suppose that concurrent glucose and drug administrations is not plausible due to unwanted chemical reactions. We propose another control strategy that administers glucose $u_G(t)$ and drug $u_D(t)$ infusions alternately. At initial time $t = 0$, glucose infusion is obtained by solving the optimal control problem using the numerical scheme FBSM for 3 hours. Next, drug infusion is attained for the next 3 hours in a similar manner. Hence, the controls $u_G(t)$ and $u_D(t)$ are applied one after the other. Subsequently, miR-451 levels are then tracked and before it crosses the threshold value, glucose infusion $u_G(t)$ and drug infusion $u_D(t)$ are again administered alternately in a similar fashion above, over the specified duration of administration. Thus, the time for the next alternating infusion is determined by tracking miR-451 levels. This strategy is referred simply as *alternating control*. This infusion protocol is shown in Fig 11(A) and 11(B). Note that glucose infusion increases miR-451 levels and drug infusion activates mTOR activities keeping AMPK down-regulated as depicted in Fig 11C. The intracellular dynamics under alternating control is illustrated in Fig 12. As shown in Fig 12A, miR-451 and mTOR levels stay above the threshold values, and $[mass_s] \approx [mass]$. Fig 12B depicts that mTOR–miR-451–AMPK trajectory are confined in proliferation region. Fig 12C exhibits the time courses of cell cycle variables under alternating control.

Comparison between control strategies

Both concomitant and alternating control strategies are able to sustain elevated miR-451 and mTOR levels above their threshold values and AMPK levels below its threshold value. It was also shown that mTOR–miR-451–AMPK trajectory is restrained in the proliferation region

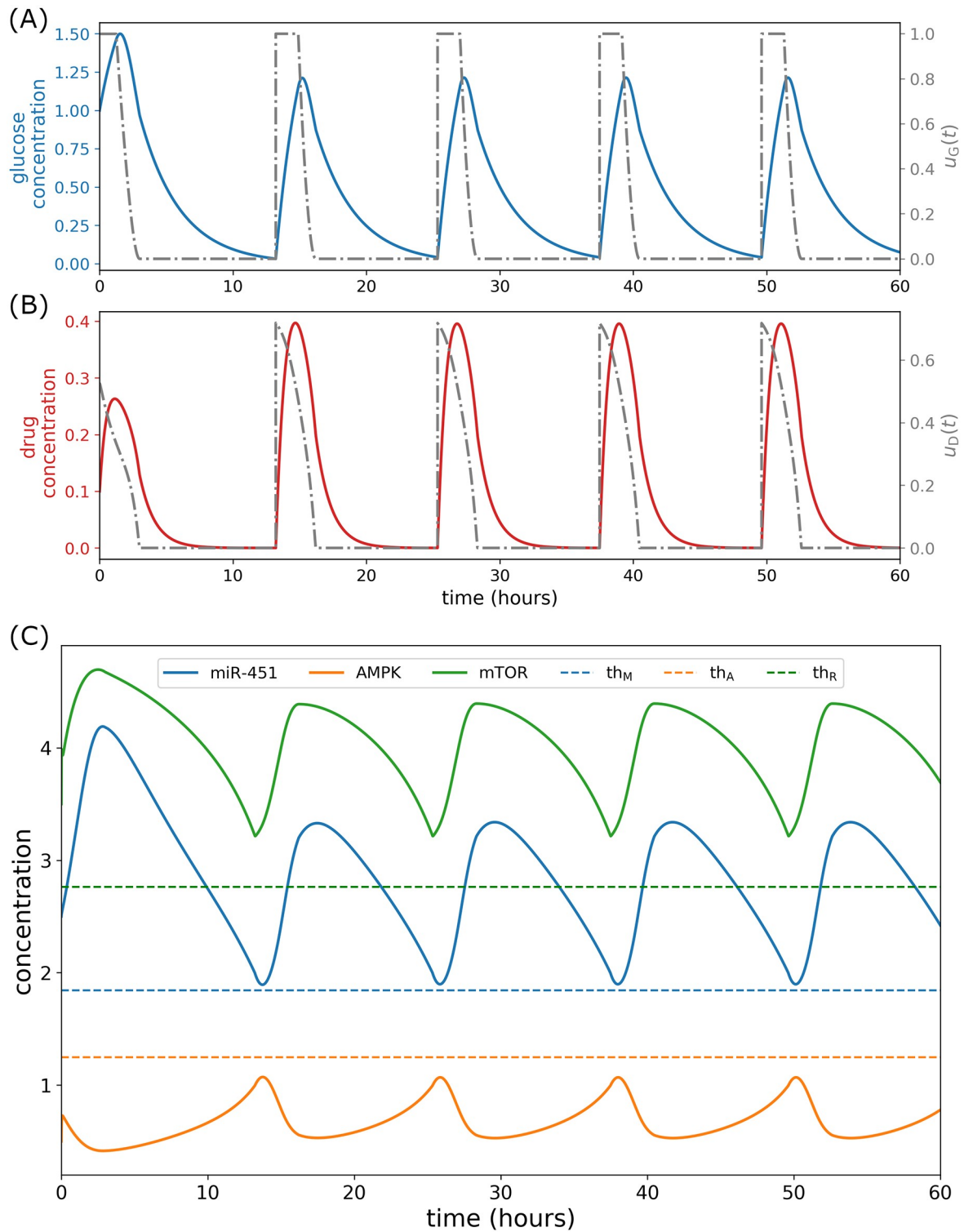


Fig 9. Concomitant glucose and drug control. (A) Glucose control and concentration levels, (B) drug control and concentration levels, and (C) concentration profiles of miR-451, AMPK complex, and mTOR under concomitant control.

<https://doi.org/10.1371/journal.pone.0215547.g009>

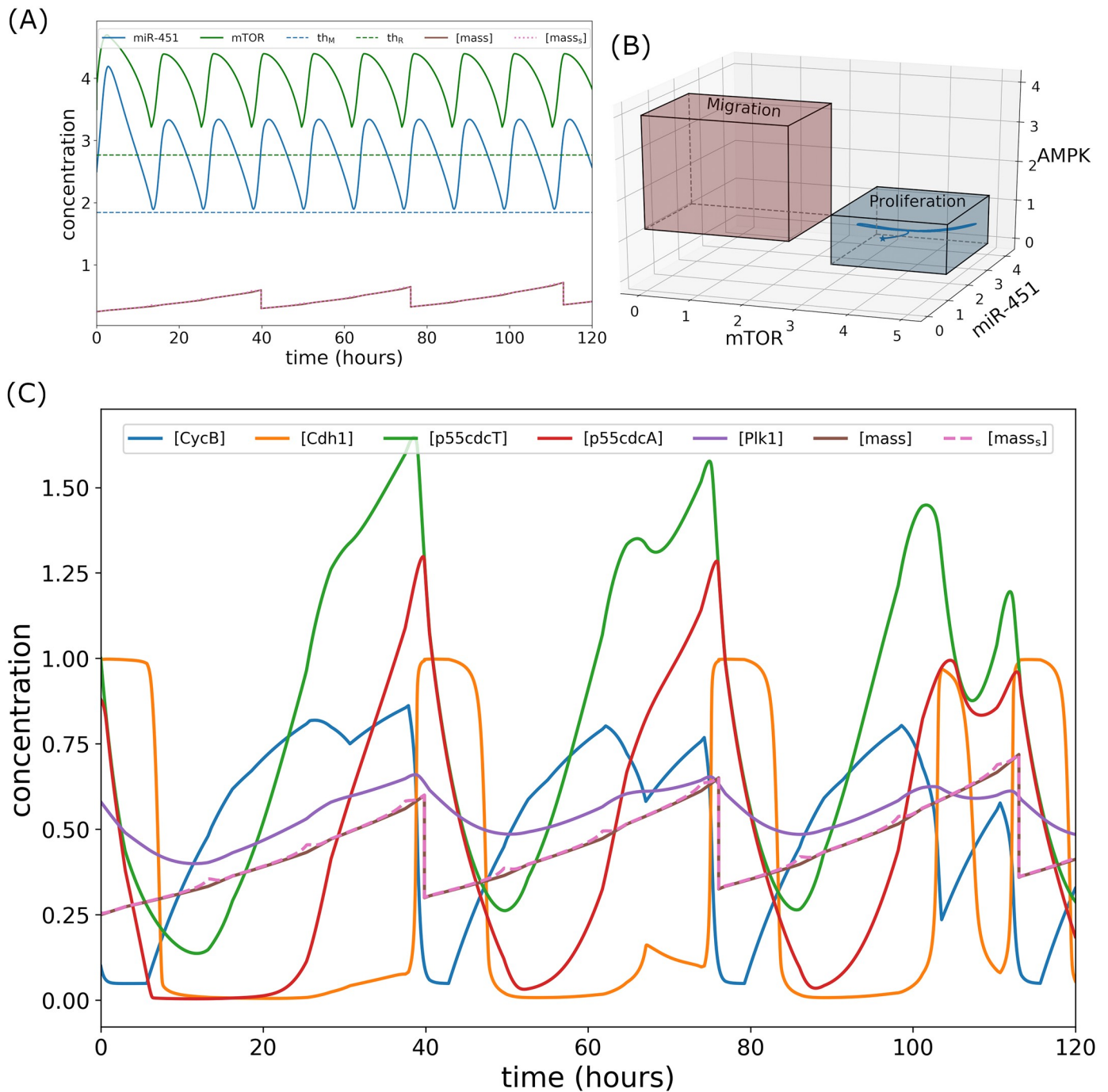


Fig 10. Intracellular dynamics under concomitant glucose and drug control. (A) Concentration profiles of miR-451 (M) and mTOR (R) above the threshold values under concomitant infusions. (B) Trajectory of mTOR–miR-451–AMPK concentration profiles restrained in the proliferation region. (C) Dynamics of intracellular proteins, mass, and mass_s of the cell cycle model in response to concomitant glucose and drug infusions.

<https://doi.org/10.1371/journal.pone.0215547.g010>

prohibiting cell migration. Further, number of cell divisions is reduced with slightly higher mass concentration before division compared to regular infusions but lower compared to constant (intermediate) high glucose concentrations. In this section, we compare the cost efficiency of the proposed strategies in terms of frequency of administration, dose per infusion, total glucose and drug amount, relative cost per infusion, and total cost incurred in the

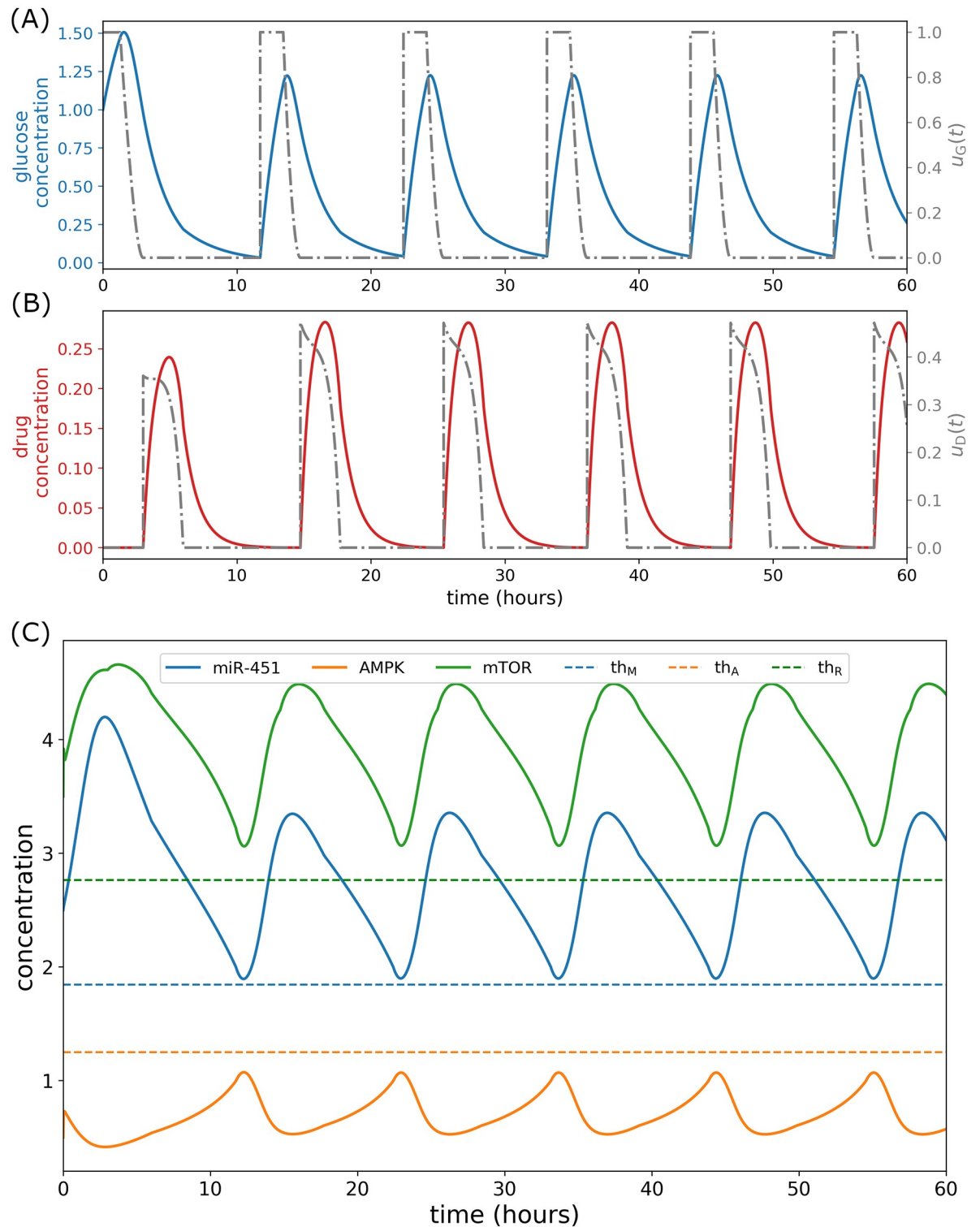


Fig 11. Alternating glucose and drug control. (A) Glucose control and concentration levels, (B) drug control and concentration levels, and (C) concentration profiles of miR-451, AMPK complex, and mTOR under alternating control.

<https://doi.org/10.1371/journal.pone.0215547.g011>

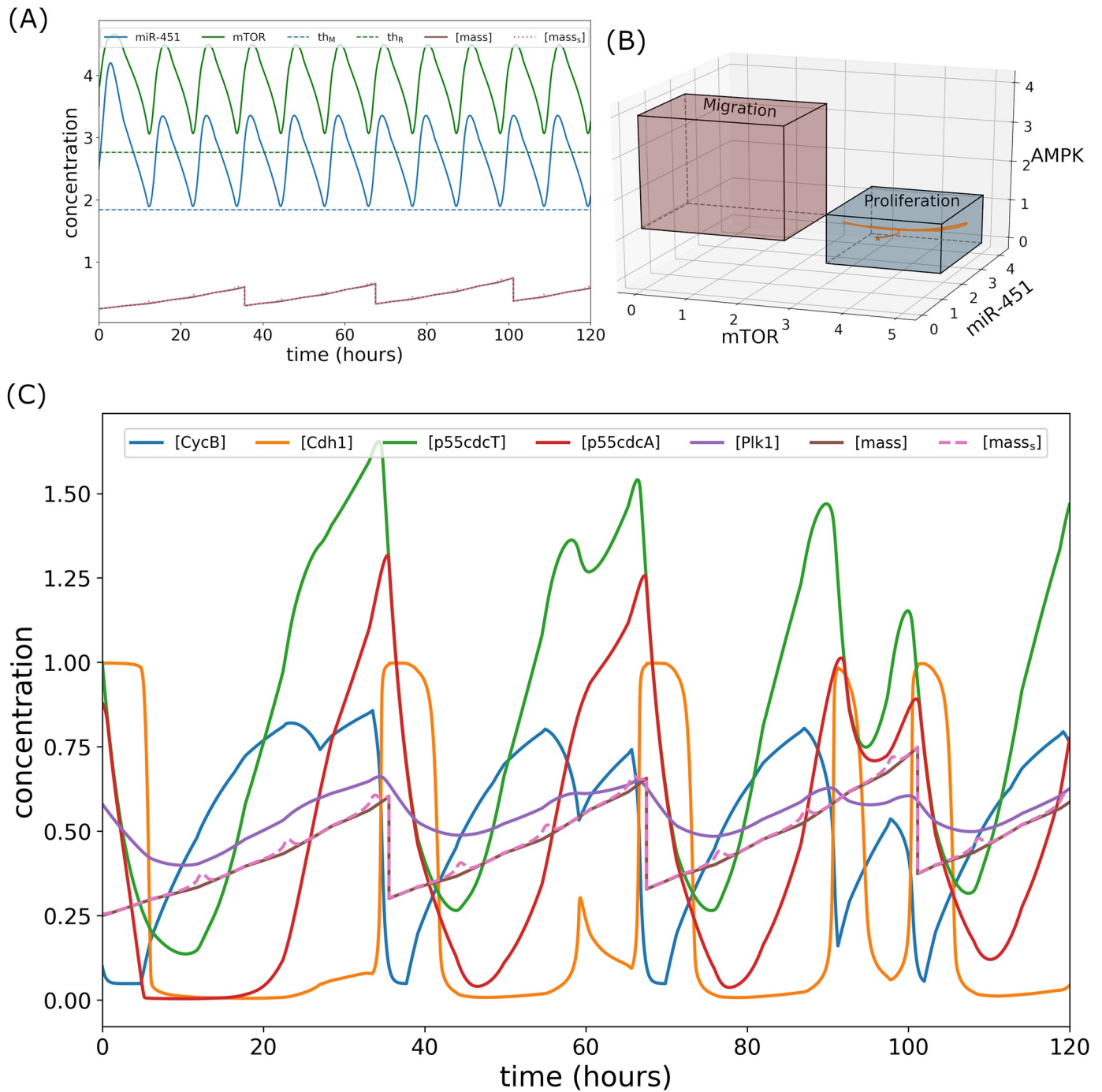


Fig 12. Intracellular dynamics under alternating glucose and drug control. (A) Concentration profiles of miR-451 (M) and mTOR (R) above the threshold values under concomitant infusions. (B) Trajectory of mTOR–miR-451–AMPK concentration profiles restrained in the proliferation region. (C) Dynamics of intracellular proteins, mass, and mass_s of the cell cycle model in response to alternating glucose and drug infusions.

<https://doi.org/10.1371/journal.pone.0215547.g012>

administrations. For the following results, the time for simulation duration is considered to be 168 hours (7days).

Recall that parameters B_1 and B_2 are the weight factors associated in our objective functional which represent the measure of costs involved in the administration of glucose $u_G(t)$

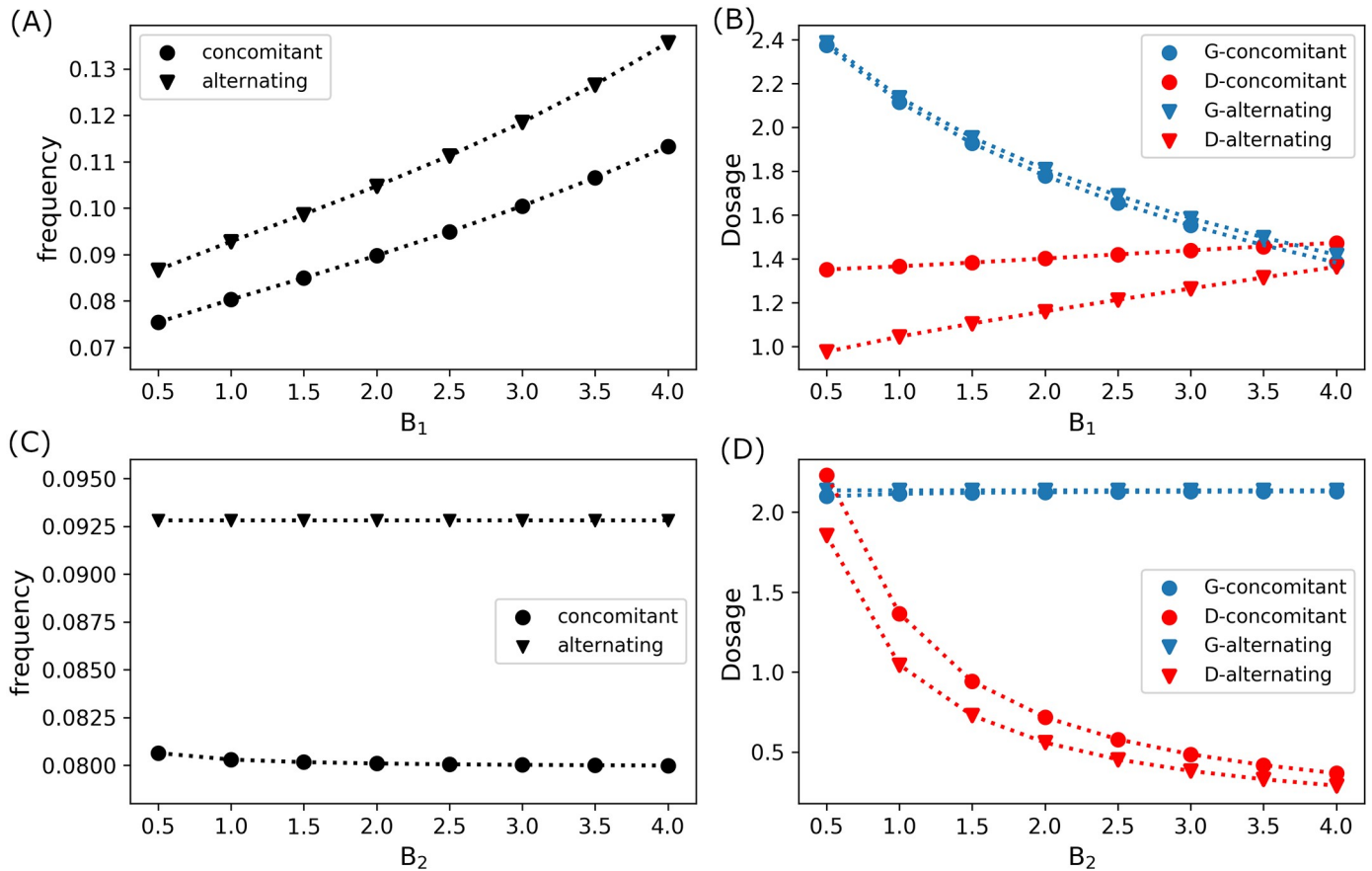


Fig 13. Frequency and dosage of optimal infusions. (A) Frequency and (B) dose per optimal infusion of concomitant (circle) and alternating (triangle) controls with fixed drug administration cost $B_2 = 1.0$ and varying glucose administration cost B_1 . (C) Frequency and (D) dose per optimal infusion of concomitant (circle) and alternating (triangle) controls with fixed glucose administration cost $B_1 = 1.0$ and varying drug administration cost B_2 .

<https://doi.org/10.1371/journal.pone.0215547.g013>

and drug $u_D(t)$ infusions, respectively, which also includes dosage, type, brand, medical fee for administration, etc. Fig 13A shows that as the cost of glucose administration becomes expensive (increasing B_1 values) with fixed drug administration cost ($B_2 = 1.0$), frequency of concomitant and alternating infusion increases. However, it should be observed that as frequency of administration increases, the optimal glucose dose per infusion decreases with drug dose per infusion increases, see Fig 13B. Increasing drug dosage compensates the decreasing glucose dosage in order to keep mTOR activities up-regulated leading to cell proliferation. On the contrary, if drug administration cost increases (increasing B_2 values) with fixed glucose administration cost ($B_1 = 1.0$), frequency of administration remains almost constant. This is depicted in Fig 13C. The glucose dose per infusion is almost the same but the drug dose per infusion decreases with increasing B_2 as illustrated in Fig 13D. Further, note that frequency of concomitant infusion control is always lower than that of alternating infusion control. In addition, drug (glucose) dose per infusion of concomitant control is always more (slightly less) than that of alternating control.

For increasing glucose administration cost (increasing B_1) with fixed drug administration cost ($B_2 = 1.0$), total amount of glucose used for both control strategies generally decrease (except for high $B_1 > 3.0$ values), as depicted in Fig 14A, while total amount of drug increases, see Fig 14B. On the other hand, when drug administration becomes expensive (increasing B_2

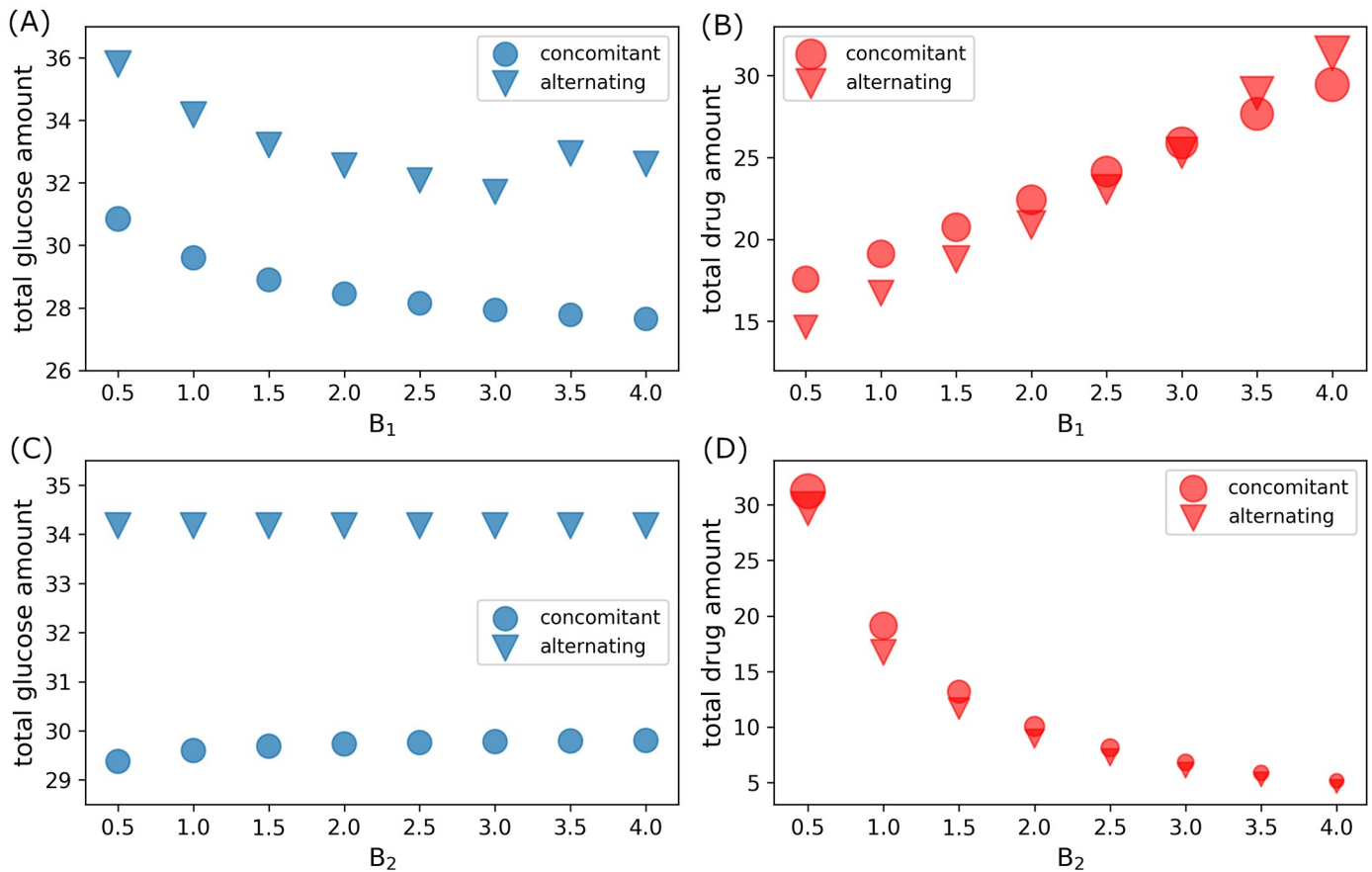


Fig 14. Total glucose and drug amount used in concomitant and alternating control infusions. (A) Total glucose and (B) drug amount used in concomitant (circle) and alternating (triangle) controls with fixed drug administration cost $B_2 = 1.0$ and varying glucose administration cost B_1 . (C) Total glucose and (D) drug amount used in concomitant (circle) and alternating (triangle) controls with fixed glucose administration cost $B_1 = 1.0$ and varying drug administration cost B_2 .

<https://doi.org/10.1371/journal.pone.0215547.g014>

values) with fixed glucose administration cost ($B_1 = 1.0$), the total amount of glucose dosage is almost constant (just slightly increasing for concomitant control) as shown in Fig 14C, but the total drug amount is decreasing as can be seen in Fig 14D. As illustrated in Fig 14, concomitant control use less total amount of glucose than that of alternating control. Contrarily, concomitant administration consumes more total drug amount as compared to that of alternating control (except possibly for high glucose administration cost, $B_1 > 3.0$, see Fig 14B).

Figs 15 and 16 reflect the relative cost per infusion and total administration cost of glucose and drug infusions incurred under concomitant and alternating controls. With fixed drug administration cost ($B_2 = 1.0$), relative glucose cost per infusion and total administration cost increases as B_1 increases. Note that alternating control cost for glucose is always higher than concomitant infusions, see Fig 15(A) and 15(B). The relative and total administration cost for concomitant infusion slightly increase as compared to alternating control as B_1 increases. Again, alternating control incur more cost for higher glucose administration cost as illustrated in Fig 15(C) and 15(D). On the other hand, when $B_1 = 1.0$ and drug administration cost (B_2) increases, the relative glucose cost per infusion and total administration cost is almost constant. This can be seen in Fig 16(A) and 16(B). Again, relative total cost for alternating control is higher than that of concomitant control. Further, as B_2 increases, relative drug cost per infusion and total administration cost decreases (Fig 16(C) and 16(D)), since total drug dosage

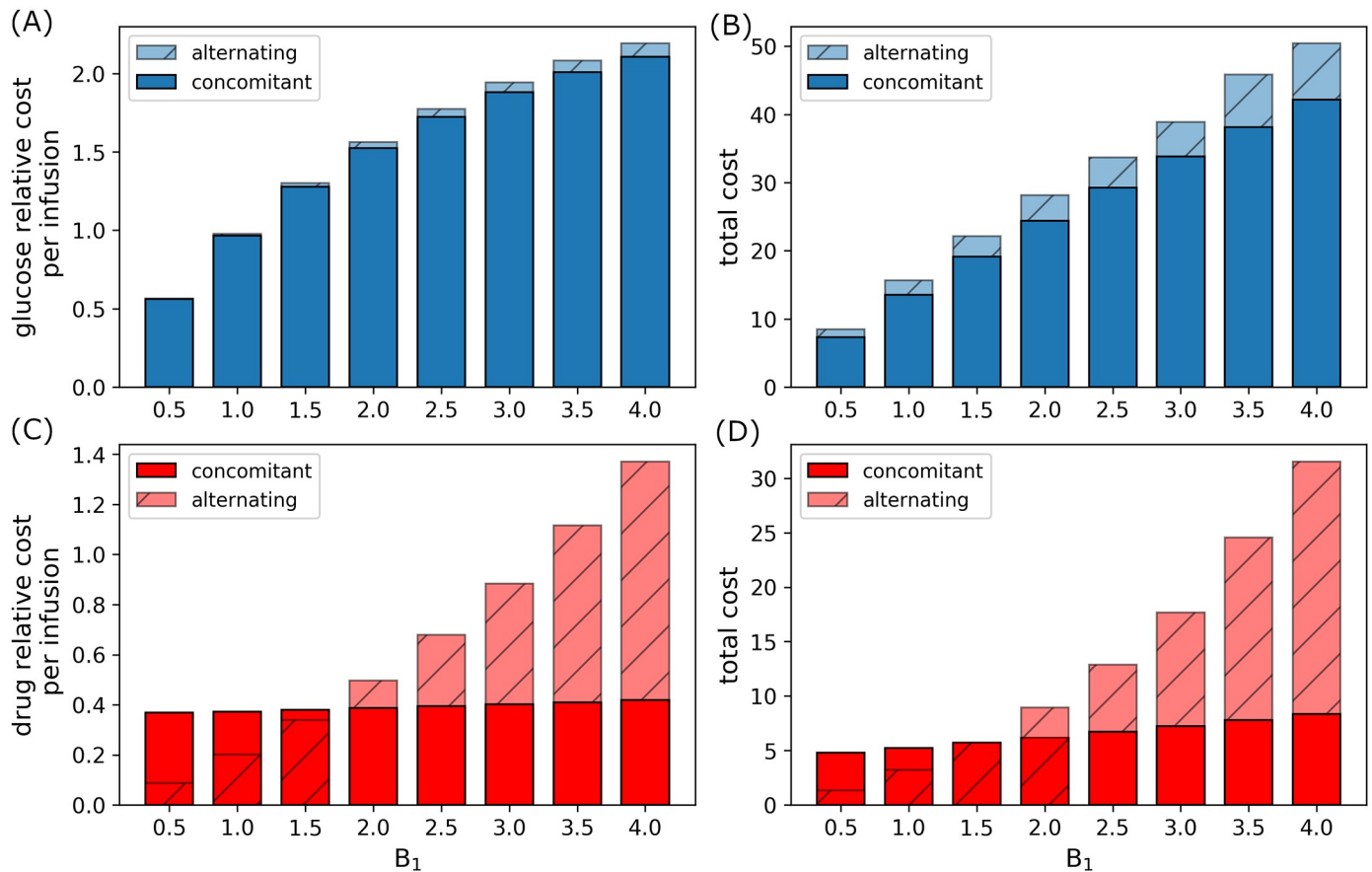


Fig 15. Relative administration cost for varying B_1 . Relative glucose administration (A) cost per infusion and (B) total cost, and relative drug administration (C) cost per infusion and (D) total cost incurred for a period of 168h (7d) for concomitant and alternating controls with increasing B_1 .

<https://doi.org/10.1371/journal.pone.0215547.g015>

also decreases as shown in Fig 14D. In this case, it can be seen that drug administration cost for alternating control is generally lower than that of concomitant control.

Observe that in Fig 17, both concomitant (blue) and alternating (orange) control trajectories in glucose–mTOR–drug space are restricted in a smaller region avoiding aggressive invasion, rapid proliferation, and unwanted drug complications. Both strategies achieved the goal of keeping mTOR (miR-451) up-regulated inducing cell proliferation and thus avoiding aggressive cell migration. It is important to note that under these proposed optimal control infusions, glucose and drug levels are regulated to prevent excessive cell division and tumor growth. As a consequence, these strategies suggest safer infusion administration preventing hyperglycemia for diabetic patients and risk of drug complications.

Table 3 provides the average frequency, dosage and relative cost of concomitant and alternating control strategies where $B_1 = B_2 = 1.0$ and simulation time is 168h (7d).

Conclusion

The periodic switching behavior of glioblastoma cells between proliferation and invasion phases is highly influenced by fluctuating glucose levels [14, 17]. In response to high glucose supply, miR-451 and mTOR are up-regulated and AMPK complex is down-regulated inducing cell growth. On the contrary, low glucose level up-regulates AMPK complex, down-regulating miR-451 and mTOR, promoting cell migration [15]. The mutual antagonistic mechanism

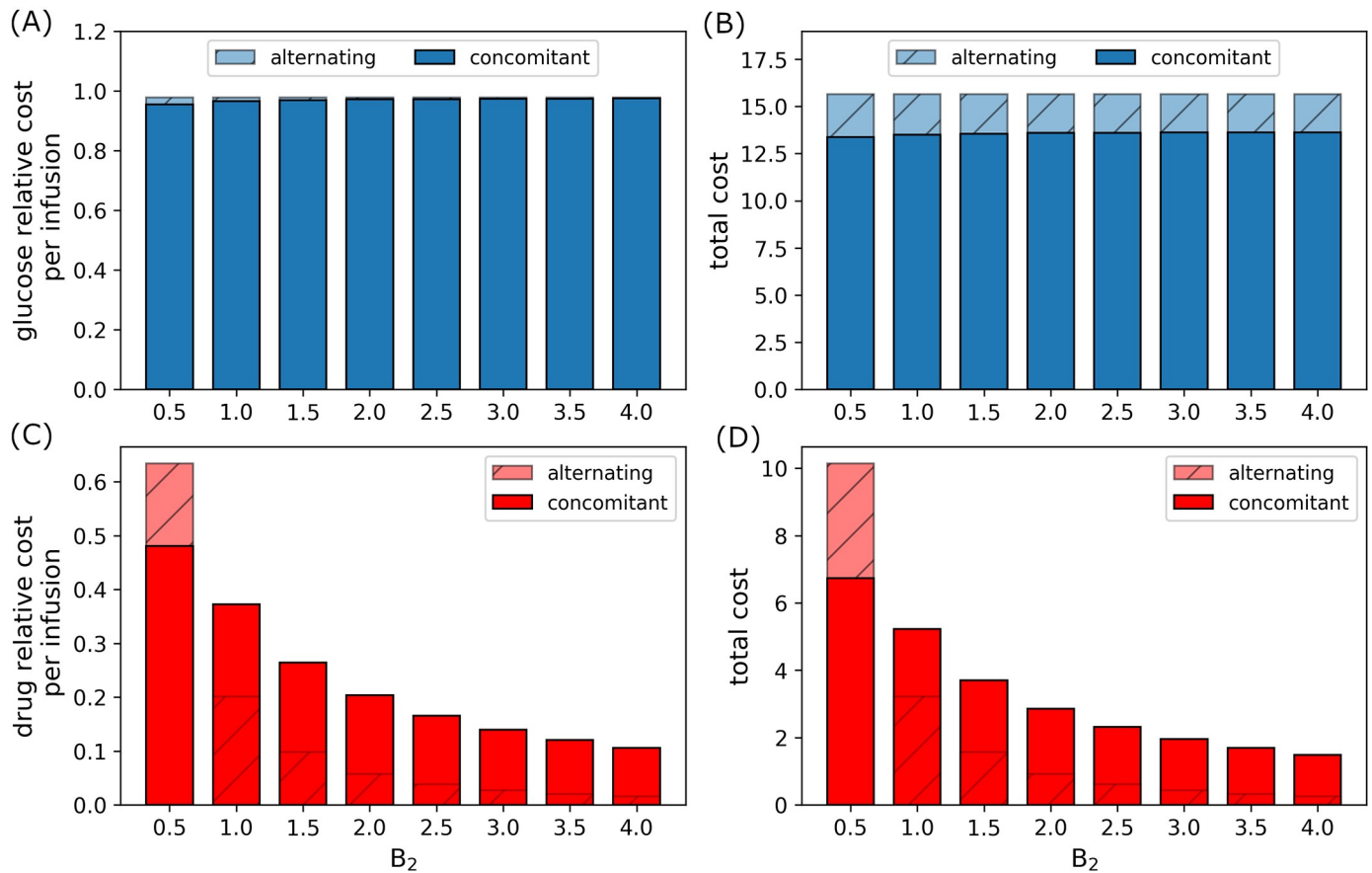


Fig 16. Relative administration cost for varying B_2 . Relative glucose administration (A) cost per infusion and (B) total cost, and relative drug administration (C) cost per infusion and (D) total cost incurred for a period of 168h (7d) for concomitant and alternating controls with increasing B_2 .

<https://doi.org/10.1371/journal.pone.0215547.g016>

between miR-451 (mTOR) and AMPK complex and the cell’s strategic metabolic adaptation support the survival of cancer cells even in a nutrient-deprived microenvironment [14, 55].

In addition to rapid proliferation of glioblastoma cells, aggressive invasion to the surrounding tissue is a major cause of treatment failure. Despite advances in medical imaging technology such as MRI and PET, glioblastoma cells can spread beyond detection leading to tumor recurrence within 2 to 3 cm of the resection cavity even after surgical removal of a malignant glioblastoma [29]. These glioma cells are capable to deform cell membrane and nucleus for cell infiltration through a narrow gap between normal glial cells in brain tissue by upregulation of myosin II along with actin bundles [26, 56]. While exact migratory patterns are still poorly understood, these invasive glioma cells prefer white matter and blood vessels [26, 57] with a wide range of speeds in the range of 5-80 $\mu\text{m}/\text{h}$ [58–61] showing sometimes saltatory patterns in the migration direction in brain [58]. Prediction of tumour invasion directions in nearby tissue may help define exact boundaries of focal treatments (surgery or radiosurgery), preventing future growth and recurrence [57]. For example, medical doctors could determine specific locations for radiation target volumes, not just using a rough estimate of 2-3 cm in all directions as a guidance as commonly done today [57].

Assuming that migratory cells are localized near the surgery site [16], one possible approach is to keep the cells in its proliferative phase preventing them from invading brain tissue in a combination with transport of therapeutic drugs near blood vessels [18]. As a result, the tumor

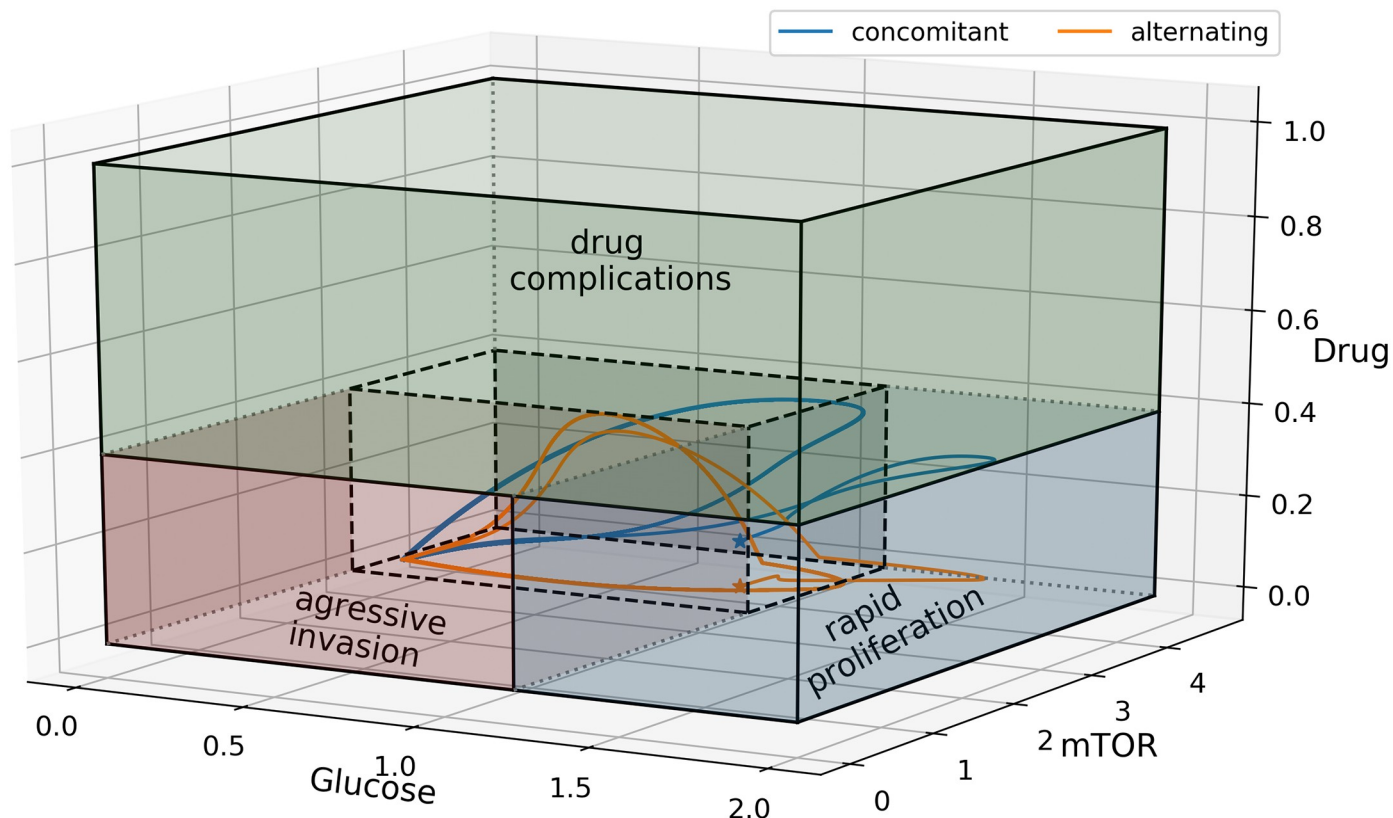


Fig 17. Glucose–mTOR–drug dynamics for concomitant and alternating controls. Concomitant (blue) and alternating (orange) control trajectories are confined in a smaller region avoiding aggressive invasion, rapid proliferation, and unwanted drug complications.

<https://doi.org/10.1371/journal.pone.0215547.g017>

mass will be visible for a succeeding surgery while killing proliferative tumor cells at the blood sites.

In this study, we considered the intracellular dynamics of the miR-451–AMPK–mTOR–cell cycle signaling pathway model developed recently by Kim *et al.* [40]. Incorporated in the model is a drug component which blocks the inhibitory pathway of mTOR by AMPK complex. This drug targets up-regulation of mTOR activities enhancing cell proliferation. The focus of the current work is to regulate up-stream signaling pathway via glucose infusion activating

Table 3. Summary for concomitant and alternating controls.

		Concomitant	Alternating
frequency	glucose infusion	0.080297	0.092806
	drug infusion	0.080297	0.092806
glucose dose	per infusion	2.114161	2.135903
	total	29.598253	34.174444
drug dose	per infusion	1.365346	1.044772
	total	19.114839	16.716352
glucose relative cost	per infusion	0.964683	0.978384
	total	13.505558	15.65414
drug relative cost	per infusion	0.372771	0.201441
	total	19.114839	16.716352

<https://doi.org/10.1371/journal.pone.0215547.t003>

miR-451, and control the down-stream pathway to cell cycle via drug infusion enhancing mTOR activities. Optimal control problem is formulated with the goal of keeping high levels of miR-451 and mTOR to induce cell growth and reduce invasion to the surrounding tissues. In the framework of optimal control theory, two administration strategies are explored to achieve the goal with minimal cost incurred in glucose and drug administrations. The control strategies investigated in this study are (1) concomitant infusion control and, and (2) alternating glucose and drug infusion control. Both strategies are able to switch on the proliferative mode of glioblastoma cells and turn off its migratory mode. Cell cycle is regulated with fewer mass divisions restricting rapid growth. Numerical results show that concomitant control had fewer infusions, lesser glucose dosage and cheaper administration cost. However, when glucose and drug poses unwanted chemical reactions during concurrent administration, alternating control would be beneficial with lower drug amount usage.

The mathematical models of the miR-451-AMPK-mTOR core control [14, 16–18, 40] are based on a ‘go-or-grow’ hypothesis and supporting experiments in GBM cells [8, 15, 19]. However, the range of bistable behavior indicates a ‘go-and-grow’ program which has been proposed for other cancers too [62]. In the glioma cases, ‘go-or-grow’ hypothesis has been long suggested [29, 55, 63–66] in addition to miR-451-induced ‘go-or-grow’ mechanism [8, 15, 19]. Glioma consists of a bulky, proliferative core in the center and highly invasive individual cells in the outer rim [55, 63, 64, 67] and sequential transition between proliferative and invasive phenotypes characterizes tumor progression and may lead to faster growth [14]. At least at the microscopic level, these migration/proliferation phenotypes appear to be mutually exclusive characteristics at different time frames [64], as suggested by in vivo imaging data of glioma cells migrating in a saltatory fashion [58]. Glioma cells was shown to pause for a short period of time (\sim an hour) for cell division before the daughter cells begin to move again [58]. Gal *et al.* [68] further experimentally observed that this phenotypic switch can happen under different extracellular environment: (i) proliferative type in soft agar via activation of Myc signaling pathways in response to hepatocyte growth factor (HGF); and (ii) infiltrative type in Matrigel through Ras signaling pathways in response to the same HGF. Recently, Dhruv *et al.* [69] also affirmed the role of activation of key molecules in dichotomy between proliferation and invasion: c-Myc and NF κ B in the proliferative core and radially dispersed, invasive region of GBM tumors, respectively. Glial cells can also interact with GBM tumor cells for phenotypic switch of GBM cells between cell migration and active proliferation [66]. Although these experiment and mathematical modeling support the ‘go-or-grow’ hypothesis, it is not certain if alternative mechanism such as ‘go-and-grow’ occurs in such a heterogenous TME in real patients [64]. Mansury *et al.* [70] for instance illustrated that individual glioma cell in a mixed group of proliferative and invasive phenotypes can depend on genotype of counter part and tumor microenvironment. In a similar conceptual studies on epithelial-to-mesenchymal transition (EMT) and mesenchymal-to-epithelial transition (MET) [45] can give a hint on the complexities of this complex regulation of those two phenotypes and glioma in TME might not possess the simple ‘go-or-grow’ dogma. Increasing number of evidences now suggest that the ‘go-or-grow’ model has similar molecular basis with EMT [64]. For instance, HGF and TGF β are major regulators of EMT, and these also provide strong stimuli of GBM invasion [71, 72] and, upregulation of MET and CD44 activities, as well as an activated NF κ B signaling pathway, was reported in both mesenchymal GBM and metastatic cancer [73–76]. All these experimental observations suggest that metastatic epithelial cancers and mesenchymal GBM drive common mechanisms that regulate the phenotypic transition between invasion and proliferation, suggesting the possibility of the ‘go-and-grow’ mechanism. The EMT paradigm in GBM has not been extensively studied as relevant to the progression of the disease due to different origin and rare

metastasis of glioma [77, 78]. Further studies and experimentation need to be done for better understanding of the fundamental principles.

In this paper, we did not take into account key microenvironmental factors such as endogenous immune dynamics including NK cells [79] and M1/M2 macrophages [72], other major signaling networks [80, 81] such as E2F and Myc [11, 82], angiogenesis [80, 83], biophysical interaction between tumor cells and blood vessels [80], ECM remodeling for therapy [81, 84–86], or growth factors [87, 88] such as epidermal growth factors [72, 89, 90], fibroblast growth factors [91], transforming growth factor- β [72, 92], and CSF-1 [72, 93, 94], that may play critical roles in proliferation, progress, aggressive invasion of gliomas and development of anti-cancer strategies [95]. For example, endogenous NK cells may interfere oncolytic virus combination therapy in GBM while exogenous NK cells increase anti-tumor efficacy [79], illustrating the complex nature of tumor microenvironment. Recently, mTOR was considered to be a master regulator of cell growth and recognized as a good therapeutic target for therapies in glioblastoma [96]. A recent study found that withaferin A and temozolomide can induce apoptosis and reduce drug resistance by G2/M cell cycle arrest through intrinsic and extrinsic apoptotic signaling pathways [97]. More detailed analysis and experiments on Akt/mTOR/PI3K are necessary. Interestingly, radiation was shown to indirectly promote the export of lactate into the extracellular space and inhibition of AMPK/NF κ B signaling pathways were involved in radiation-induced invasion of cancer cells [98]. On the other hand, M2 microglia/macrophages induce matrix remodeling and glioma cell invasion [72, 99–101]. Since PI3K signaling was shown to contribute to M2-polarization of these tumor associated macrophages (TAMs) [102] and PI3K binding to CSF1R was shown to enhance spreading of macrophages, thus promoting glioma cell invasion [103]. Therefore, better understanding of these PI3K-mTOR-CSF1R signaling networks in macrophages would lead to development of blocking aggressive infiltration of cancer cells. Signaling pathways of apoptosis and necroptosis are important parts of oncolytic virus (OVs) therapy [104, 105]. Tumor extracellular matrix (ECM) plays a significant role in regulation of glioma invasion in brain tissue as well as OV spread [106]. For example, CSPGs, one of major tumor ECM in brain can characterize the invasive and non-invasive gliomas in a complex TME where microglia and astrocytes mechanically interact with CSPGs and tumor cells [40, 107–109]. Hybrid models [56, 110–112] and its associated optimal control strategies can be adapted to take into account this important intracellular signaling as well as cell population dynamics and tissue dynamics. Better understanding of various roles of these components in tumor microenvironment may provide better anti-invasion strategies of glioma cells.

However, our mathematical model in this work is a first step toward further experimental/clinical investigation and more optimal anti-invasion strategies of GBM by incorporating these microenvironmental components. We will address these issues in future work.

Supporting information

S1 Appendix. Optimal control problem. Formulation of the optimal control problem for concomitant and alternating glucose and drug infusion.
(PDF)

Acknowledgments

This work is resulted from the Konkuk University research support program (E.J.). This paper is also supported by the Korea National Research Foundation (NRF) grant funded by the Korean government (MEST): NRF- 2017R1A2B2004651 (E.J.) and the Basic Science Research

Program through National Research Foundation of Korea (NRF) funded by Ministry of Science, ICT and Future Planning: (2018R1A2B6007288) (Y.K.). This work was funded by the University of the Philippines System Enhanced Creative Work and Research Grant (ECWRG 2016-1-030) (A.d.l.R). K.J.A.P. is supported by the University of the Philippines-Office of International Linkages-Continuous Operational and Outcomes-based Partnership for Excellence in Research and Academic Training Enhancement (UP-OIL-COOPERATE) grant and the Department of Science and Technology-Accelerated Science and Technology Human Resource Development Program-National Science Consortium (DOST-ASTHRDP-NSC) Scholarship.

Author Contributions

Conceptualization: Eunok Jung, Aurelio A. de los Reyes V, Yangjin Kim.

Formal analysis: Kurt Jan A. Pumares.

Investigation: Aurelio A. de los Reyes V, Kurt Jan A. Pumares.

Methodology: Eunok Jung, Aurelio A. de los Reyes V, Kurt Jan A. Pumares.

Supervision: Eunok Jung, Yangjin Kim.

Validation: Eunok Jung, Aurelio A. de los Reyes V.

Visualization: Aurelio A. de los Reyes V.

Writing – original draft: Aurelio A. de los Reyes V, Kurt Jan A. Pumares, Yangjin Kim.

Writing – review & editing: Yangjin Kim.

References

1. Chintala SK, Tonn JC, Rao JS. Matrix metalloproteinases and their biological function in human gliomas. *Int J Dev Neurosci.* 1999; 17(5-6):495–502. [https://doi.org/10.1016/S0736-5748\(99\)00010-6](https://doi.org/10.1016/S0736-5748(99)00010-6) PMID: 10571411
2. Furnari FB, Fenton T, Bachoo RM, Mukasa A, Stommel JM, Stegh A, et al. Malignant astrocytic glioma: genetics, biology, and paths to treatment. *Genes Dev.* 2007; 21(21):2683–710. <https://doi.org/10.1101/gad.1596707> PMID: 17974913
3. Davis FG, McCarthy BJ. Current epidemiological trends and surveillance issues in brain tumors. *Expert Rev Anticancer Ther.* 2001; 1(3):395–401. <https://doi.org/10.1586/14737140.1.3.395> PMID: 12113106
4. Warburg O. On the origin of cancer cells. *Science.* 1956; 123(3191):309–14. <https://doi.org/10.1126/science.123.3191.309> PMID: 13298683
5. Heiden MG, Cantley LC, Thompson CB. Understanding the Warburg effect: the metabolic requirements of cell proliferation. *Science.* 2009; 324(5930):1029–33. <https://doi.org/10.1126/science.1160809>
6. Kim JW, Dang CV. Cancer's molecular sweet tooth and the Warburg effect. *Cancer Res.* 2006; 66(18):8927–30. <https://doi.org/10.1158/0008-5472.CAN-06-1501> PMID: 16982728
7. Xu RH, Pelicano H, Zhou Y, Carew JS, Feng L, Bhalla KN, et al. Inhibition of glycolysis in cancer cells: a novel strategy to overcome drug resistance associated with mitochondrial respiratory defect and hypoxia. *Cancer Res.* 2005; 65(2):613–21. PMID: 15695406
8. Godlewski J, Nowicki MO, Bronisz A, Palatini GN, Lay MD, Brocklyn JV, et al. MicroRNA-451 regulates LKB1/AMPK signaling and allows adaptation to metabolic stress in glioma cells. *Molecular Cell.* 2010; 37:620–632. <https://doi.org/10.1016/j.molcel.2010.02.018> PMID: 20227367
9. Hardie DG. AMP-activated/SNF1 protein kinases: conserved guardians of cellular energy. *Nat Rev Mol Cell Biol.* 2007; 8(10):774–85. <https://doi.org/10.1038/nrm2249> PMID: 17712357
10. Bartel DP. MicroRNAs: target recognition and regulatory functions. *Cell.* 2009; 136(2):215–33. <https://doi.org/10.1016/j.cell.2009.01.002> PMID: 19167326

11. Aguda BD, Kim Y, Piper-Hunter MG, Friedman A, Marsh CB. MicroRNA regulation of a cancer network: Consequences of the feedback loops involving miR-17-92, E2F, and Myc. *Proceedings of the National Academy of Sciences*. 2008; 105(50):19678–19683. <https://doi.org/10.1073/pnas.0811166106>
12. Esquela-Kerscher A, Slack FJ. OncomiRs—microRNAs with a role in cancer. *Nat Rev Cancer*. 2006; 6(4):259–69. <https://doi.org/10.1038/nrc1840> PMID: 16557279
13. Godlewski J, Nowicki MO, Bronisz A, Williams S, Otsuki A, Nuovo G, et al. Targeting of the BMI-1 oncogene/stem cell renewal factor by microRNA-128 inhibits glioma proliferation and self-renewal. *Cancer Res*. 2008; 68(22):9125–30. <https://doi.org/10.1158/0008-5472.CAN-08-2629> PMID: 19010882
14. Kim Y, Roh S, Lawler S, Friedman A. miR451 and AMPK Mutual Antagonism in Glioma Cell Migration and Proliferation: A Mathematical Model. *PLoS One*. 2011; 6(12):1–10. <https://doi.org/10.1371/journal.pone.0028293>
15. Godlewski J, Bronisz A, Nowicki MO, Chiocca EA, Lawler S. microRNA-451: A conditional switch controlling glioma cell proliferation and migration. *Cell Cycle*. 2010; 9(14):2742–8. <https://doi.org/10.4161/cc.9.14.12248> PMID: 20647762
16. Kim Y. Regulation of Cell Proliferation and Migration in Glioblastoma: New Therapeutic Approach. *Frontiers in Oncology*. 2013; 3:53. <https://doi.org/10.3389/fonc.2013.00053> PMID: 23508546
17. Kim Y, Roh S. A hybrid model for cell proliferation and migration in glioblastoma. *Discrete & Continuous Dynamical Systems—B*. 2013; 18:969–1015. <https://doi.org/10.3934/dcdsb.2013.18.969>
18. Kim Y, Powathil G, Kang H, Trucu D, Kim H, Lawler S, et al. Strategies of Eradicating Glioma Cells: A Multi-Scale Mathematical Model with MiR-451-AMPK-mTOR Control. *PLoS One*. 2015; 10(1):1–30. <https://doi.org/10.1371/journal.pone.0114370>
19. Ansari KI, Ogawa D, Rooj AK, Lawler SE, Krichevsky AM, Johnson MD, et al. Glucose-based regulation of miR-451/AMPK signaling depends on the OCT1 transcription factor. *Cell Rep*. 2015; 11(6):902–909. <https://doi.org/10.1016/j.celrep.2015.04.016> PMID: 25937278
20. Schwartz GK, Shah MA. Targeting the cell cycle: a new approach to cancer therapy. *J Clin Oncol*. 2005; 23:9408–9421. <https://doi.org/10.1200/JCO.2005.01.5594> PMID: 16361640
21. Douglas RM, Haddad GG. Genetic models in applied physiology: invited review: effect of oxygen deprivation on cell cycle activity: a profile of delay and arrest. *J Appl Physiol*. 2003; 94:2068–2083. PMID: 12679355
22. Garrett MD, Fattaey A. CDK inhibition and cancer therapy. *Curr Opin Genet Dev*. 1999; 9:104–111. [https://doi.org/10.1016/S0959-437X\(99\)80015-X](https://doi.org/10.1016/S0959-437X(99)80015-X) PMID: 10072351
23. Tyson JJ, Novak B. Regulation of the eukaryotic cell cycle: molecular antagonism, hysteresis, and irreversible transitions. *J Theor Biol*. 2001; 210:249–263. <https://doi.org/10.1006/jtbi.2001.2293> PMID: 11371178
24. Novak B, Tyson JJ. Modelling the controls of the eukaryotic cell cycle. *Biochem Soc Trans*. 2003; 31:1526–1529. PMID: 14641104
25. Holland EC. Glioblastoma multiforme: the terminator. *Proc Natl Acad Sci U S A*. 2000; 97(12):6242–4. <https://doi.org/10.1073/pnas.97.12.6242> PMID: 10841526
26. Beadle C, Assanah MC, Monzo P, Vallee R, Rosenfield SS, Canoll P. The role of myosin II in glioma invasion of the brain. *Mol Biol Cell*. 2008; 19:3357–3368. <https://doi.org/10.1091/mbc.E08-03-0319> PMID: 18495866
27. Claes A, Idema AJ, Wesseling P. Diffuse glioma growth: a guerilla war. *Acta Neuropathologica*. 2007; 114(5):443–458. <https://doi.org/10.1007/s00401-007-0293-7> PMID: 17805551
28. Wesseling P, Kros JM, Jeuken JWM. The pathological diagnosis of diffuse gliomas: towards a smart synthesis of microscopic and molecular information in a multidisciplinary context. *Diagnostic Histopathology*. 2011; 17(11):486–494. <https://doi.org/10.1016/j.mpdhp.2011.08.005>
29. Giese A, Bjerkvig R, Berens ME, Westphal M. Cost of migration: invasion of malignant gliomas and implications for treatment. *J Clin Oncol*. 2003; 21(8):1624–36. <https://doi.org/10.1200/JCO.2003.05.063> PMID: 12697889
30. Joshi HR. Optimal control of an HIV immunology model. *Optimal Control Applications and Methods*. 2002; 23(4):199–213. <https://doi.org/10.1002/oca.710>
31. Kwon HD. Optimal treatment strategies derived from a HIV model with drug-resistant mutants. *Applied Mathematics and Computation*. 2007; 188(2):1193–1204. <https://doi.org/10.1016/j.amc.2006.10.071>
32. Okusun KO, Makinde OD, Takaidza I. Impact of optimal control on the treatment of HIV/AIDS and screening of unaware infectives. *Applied Mathematical Modelling*. 2013; 37(6):3802–3820. <https://doi.org/10.1016/j.apm.2012.08.004>

33. Silva CJ, Torres DFM. Modeling and optimal control of HIV/AIDS prevention through PrEP. *Discrete & Continuous Dynamical Systems—S*. 2018; 11(1):119–141. <https://doi.org/10.3934/dcdss.2018008>
34. Jung E, Lenhart S, Feng Z. Optimal control of treatments in a two-strain tuberculosis model. *Discrete & Continuous Dynamical Systems—B*. 2002; 2(4):473–482. <https://doi.org/10.3934/dcdsb.2002.2.473>
35. Whang S, Choi S, Jung E. A dynamic model for tuberculosis transmission and optimal treatment strategies in South Korea. *Journal of Theoretical Biology*. 2011; 279(1):120–131. <https://doi.org/10.1016/j.jtbi.2011.03.009> PMID: 21439972
36. Kim S, de los Reyes AA, Jung E. Mathematical model and intervention strategies for mitigating tuberculosis in the Philippines. *Journal of Theoretical Biology*. 2018; 443:100–112. <https://doi.org/10.1016/j.jtbi.2018.01.026> PMID: 29407656
37. Jung E, Babbs CF, Lenhart S, Protopopescu VA. Optimal Strategy for Cardiopulmonary Resuscitation with Continuous Chest Compression. *Academic Emergency Medicine*. 2006; 13(7):715–721. <https://doi.org/10.1197/j.aem.2006.03.550> PMID: 16723728
38. Jung E, Lenhart S, Protopopescu V, Babbs C. Optimal control applied to a thoraco-abdominal CPR model. *Mathematical Medicine and Biology: A Journal of the IMA*. 2008; 25(2):157–170. <https://doi.org/10.1093/imammb/dqn009> PMID: 18515260
39. de los Reyes V AA, Jung E, Kim Y. Optimal control strategies of eradicating invisible glioblastoma cells after conventional surgery. *Journal of The Royal Society Interface*. 2015; 12(106). <https://doi.org/10.1098/rsif.2014.1392>
40. Kim Y, Kang H, Powathil G, Kim H, Trucu D, Lee W, et al. Role of extracellular matrix and microenvironment in regulation of tumor growth and LAR-mediated invasion in glioblastoma. *PLoS One*. 2018; 13(10):1–40. <https://doi.org/10.1371/journal.pone.0204865>
41. Powathil GG, Gordon KE, Hill LA, Chaplain MA. Modelling the effects of cell-cycle heterogeneity on the response of a solid tumour to chemotherapy: Biological insights from a hybrid multiscale cellular automaton model. *J Theor Biol*. 2012; 308:1–19. <https://doi.org/10.1016/j.jtbi.2012.05.015> PMID: 22659352
42. Gardner T, Cantor C, Collins J. Construction of a genetic toggle switch in *E. coli*. *Nature*. 2000; 403:339–342. <https://doi.org/10.1038/35002131> PMID: 10659857
43. Macia J, Widder S, Sole R. Why are cellular switches Boolean? General conditions for multistable genetic circuits. *J Theor Biol*. 2009; 261(1):126–35. <https://doi.org/10.1016/j.jtbi.2009.07.019> PMID: 19632240
44. Jia D, Jolly MK, Harrison W, Boareto M, Ben-Jacob E, Levine H. Operating principles of tristable circuits regulating cellular differentiation. *Phys Biol*. 2017; 14(3):035007. <https://doi.org/10.1088/1478-3975/aa6f90> PMID: 28443829
45. Lu M, Jolly MK, Levine H, Onuchic JN, Ben-Jacob E. MicroRNA-based regulation of epithelial-hybrid-mesenchymal fate determination. *Proc Natl Acad Sci USA*. 2013; 110(45):18144–9. <https://doi.org/10.1073/pnas.1318192110> PMID: 24154725
46. Dhooge A, Govaerts W, Kuznetsov YA. MATCONT: A Matlab Package for Numerical Bifurcation Analysis of ODEs. *SIGSAM Bull*. 2004; 38(1):21–22. <https://doi.org/10.1145/980175.980184>
47. Gaetano AD, Arino O. Mathematical modelling of the intravenous glucose tolerance test. *J Math Biol*. 2000; 40:136–168. <https://doi.org/10.1007/s002850050007> PMID: 10743599
48. Crute BE, Seefeld K, Gamble J, Kemp BE, Witters LA. Functional domains of the alpha1 catalytic subunit of the AMP-activated protein kinase. *J Biol Chem*. 1998; 273(52):35347–54. <https://doi.org/10.1074/jbc.273.52.35347> PMID: 9857077
49. Gantier MP, McCoy CE, Rusinova I, Saulep D, Wang D, Xu D, et al. Analysis of microRNA turnover in mammalian cells following Dicer1 ablation. *Nucleic Acids Res*. 2011; 39(13):5692–703. <https://doi.org/10.1093/nar/gkr148> PMID: 21447562
50. Gordon K. Mathematical modelling of cell-cycle-dependent chemotherapy drugs-implications for cancer treatment. PhD Thesis, University of Dundee, Dundee. 2006.
51. Fleming WH, Rishel RW. *Deterministic and Stochastic Optimal Control*. vol. 1 of *Stochastic Modelling and Applied Probability*. 1st ed. Springer-Verlag New York; 1975.
52. Pontryagin LS. *Mathematical Theory of Optimal Processes*. *Classics of Soviet Mathematics*. Taylor & Francis; 1987. Available from: <https://books.google.co.kr/books?id=kwzq0F4cBVAC>.
53. McAsey M, Mou L, Han W. Convergence of the forward-backward sweep method in optimal control. *Computational Optimization and Applications*. 2012; 53(1):207–226. <https://doi.org/10.1007/s10589-011-9454-7>
54. Marino S, Hogue IB, Ray CJ, Kirschner DE. A methodology for performing global uncertainty and sensitivity analysis in systems biology. *J Theor Biol*. 2008; 254(1):178–196. <https://doi.org/10.1016/j.jtbi.2008.04.011> PMID: 18572196

55. Kim Y, Lawler S, Nowicki MO, Chiocca EA, Friedman A. A mathematical model of Brain tumor: pattern formation of glioma cells outside the tumor spheroid core. *J Theor Biol.* 2009; 260:359–371. <https://doi.org/10.1016/j.jtbi.2009.06.025> PMID: 19596356
56. Lee W, Lim S, Kim Y. The role of myosin II in glioma invasion: A mathematical model. *PLoS One.* 2017; 12(2):e0171312. <https://doi.org/10.1371/journal.pone.0171312> PMID: 28166231
57. Esmaeili M, Stensjoen AL, Berntsen EM, Solheim O, Reinertsen I. The Direction of Tumour Growth in Glioblastoma Patients. *Sci Rep.* 2018; 8(1):1199. <https://doi.org/10.1038/s41598-018-19420-z> PMID: 29352231
58. Farin A, Suzuki SO, Weiker M, Goldman JE, Bruce JN, Canoll P. Transplanted glioma cells migrate and proliferate on host brain vasculature: a dynamic analysis. *Glia.* 2006; 53(8):799–808. <https://doi.org/10.1002/glia.20334> PMID: 16541395
59. Kim HD, Guo TW, Wu AP, Wells A, Gertler FB, Lauffenburger DA. Epidermal growth factor-induced enhancement of glioblastoma cell migration in 3D arises from an intrinsic increase in speed but an extrinsic matrix and proteolysis-dependent increase in persistence. *Mol Biol Cell.* 2008; 19:4249–4259. <https://doi.org/10.1091/mbc.E08-05-0501> PMID: 18632979
60. Sen S, Dong M, Kumar S. Isoform-specific contributions of a-cctinin to glioma cell mechanobiology. *PLoS One.* 2009; 4(12):e8427. <https://doi.org/10.1371/journal.pone.0008427> PMID: 20037648
61. Kaufman LJ, Brangwynne CP, Kasza KE, Filippidi E, Gordon VD, Deisboeck TS, et al. Glioma expansion in collagen I matrices: analyzing collagen concentration-dependent growth and motility patterns. *Biophys J BioFAST.* 2005; 89:635–650. <https://doi.org/10.1529/biophysj.105.061994>
62. Jolly MK, Ware KE, Gilja S, Somarelli JA, Levine H. EMT and MET: necessary or permissive for metastasis? *Mol Oncol.* 2017; 11(7):755–769. <https://doi.org/10.1002/1878-0261.12083> PMID: 28548345
63. Stein AM, Demuth T, Mobley D, Berens M, Sander LM. A mathematical model of glioblastoma tumor spheroid invasion in a three-dimensional in vitro experiment. *Biophys J.* 2007; 92(1):356–65. <https://doi.org/10.1529/biophysj.106.093468> PMID: 17040992
64. Xie Q, Mittal S, Berens ME. Targeting adaptive glioblastoma: an overview of proliferation and invasion. *Neuro Oncol.* 2014; 16(12):1575–84. <https://doi.org/10.1093/neuonc/nou147> PMID: 25082799
65. Lamszus K, MD, Kathagen A, Holz M, Schulte A, Westphal M. GO OR GROW—LINKS BETWEEN CELLULAR FUNCTION, GLUCOSE METABOLISM AND GLIOMA MICROENVIRONMENT. *Neuro Oncol.* 2014; 16(Suppl 3):iii6. <https://doi.org/10.1093/neuonc/nou206.19>
66. Oliveira AI, Anjo SI, de Castro JV, Serra SC, Salgado AJ, Manadas B, et al. Crosstalk between glial and glioblastoma cells triggers the go-or-grow phenotype of tumor cells. *Cell Commun Signal.* 2017; 15(1):37. <https://doi.org/10.1186/s12964-017-0194-x> PMID: 28969644
67. Khain E, Sander LM. Dynamics and pattern formation in invasive tumor growth. *Phys Rev Lett.* 2006; 96(18):188103. <https://doi.org/10.1103/PhysRevLett.96.188103> PMID: 16712401
68. Gao CF, Xie Q, Su YL, Koeman J, Khoo SK, Gustafson M, et al. Proliferation and invasion: plasticity in tumor cells. *Proc Natl Acad Sci USA.* 2005; 102(30):10528–10533. <https://doi.org/10.1073/pnas.0504367102> PMID: 16024725
69. Dhruv HD, Winslow WSM, Armstrong B, Tuncali S, Eschbacher J, Kislin K, et al. Reciprocal activation of transcription factors underlies the dichotomy between proliferation and invasion of glioma cells. *PLoS One.* 2013; 8(8):e72134. <https://doi.org/10.1371/journal.pone.0072134> PMID: 23967279
70. Mansury Y, Diggory M, Deisboeck TS. Evolutionary game theory in an agent-based brain tumor model: exploring the Genotype-Phenotype link. *J Theor Biol.* 2006; 238:146–156. <https://doi.org/10.1016/j.jtbi.2005.05.027> PMID: 16081108
71. Polyak K, Weinberg RA. Transitions between epithelial and mesenchymal states: acquisition of malignant and stem cell traits. *Nature Reviews Cancer.* 2009; 9(4):265–273. <https://doi.org/10.1038/nrc2620> PMID: 19262571
72. Kim Y, Jeon H, Othmer HG. The role of the tumor microenvironment in glioblastoma: A mathematical model. *IEEE Trans Biomed Eng.* 2017; 64(3):519–527. <https://doi.org/10.1109/TBME.2016.2637828> PMID: 27959794
73. Roussos ET, Keckesova Z, Haley JD, Epstein DM, Weinberg RA, Condeelis JS. AACR special conference on epithelial-mesenchymal transition and cancer progression and treatment. *Cancer Res.* 2010; 70(19):7360–4. <https://doi.org/10.1158/0008-5472.CAN-10-1208> PMID: 20823151
74. Knudsen BS, Woude GV. Showering c-MET-dependent cancers with drugs. *Curr Opin Genet Dev.* 2008; 18(1):87–96. <https://doi.org/10.1016/j.gde.2008.02.001> PMID: 18406132
75. Raychaudhuri B, Han Y, Lu T, Vogelbaum MA. Aberrant constitutive activation of nuclear factor kappaB in glioblastoma multiforme drives invasive phenotype. *J Neurooncol.* 2007; 85(1):39–47. <https://doi.org/10.1007/s11060-007-9390-7> PMID: 17479228

76. Chaffer CL, Brueckmann I, Scheel C, Kaestli AJ, Wiggins PA, Rodrigues LO, et al. Normal and neoplastic nonstem cells can spontaneously convert to a stem-like state. *Proc Natl Acad Sci U S A*. 2011; 108(19):7950–5. <https://doi.org/10.1073/pnas.1102454108> PMID: 21498687
77. Krol I, Castro-Giner F, Maurer M, Gkountela S, Szczurba BM, Scherrer R, et al. Detection of circulating tumour cell clusters in human glioblastoma. *Br J Cancer*. 2018; 119(4):487–491. <https://doi.org/10.1038/s41416-018-0186-7> PMID: 30065256
78. Goodwin CR, Liang L, Abu-Bonsrah N, Hdeib A, Elder BD, Kosztowski T, et al. Extraneural Glioblastoma Multifforme Vertebral Metastasis. *World Neurosurg*. 2016; 89:578–582. <https://doi.org/10.1016/j.wneu.2015.11.061> PMID: 26704201
79. Kim Y, Yoo JY, Lee TJ, Liu J, Yu J, Caligiuri MA, et al. Complex role of NK cells in regulation of oncolytic virus-bortezomib therapy. *Proc Natl Acad Sci USA*. 2018; 115(19):4927–4932. <https://doi.org/10.1073/pnas.1715295115> PMID: 29686060
80. Griveau A, Seano G, Shelton SJ, Kupp R, Jahangiri A, Obernier K, et al. A Glial Signature and Wnt7 Signaling Regulate Glioma-Vascular Interactions and Tumor Microenvironment. *Cancer Cell*. 2018; online pii: S1535–6108(18)30125–9. <https://doi.org/10.1016/j.ccell.2018.03.020> PMID: 29681511
81. Rajesh Y, Biswas A, Mandal M. Glioma progression through the prism of heat shock protein mediated extracellular matrix remodeling and epithelial to mesenchymal transition. *Exp Cell Res*. 2017; 359(2):299–311. <https://doi.org/10.1016/j.yexcr.2017.08.032> PMID: 28844885
82. Aguda BD, Kim Y, Kim HS, Friedman A, Fine H. Qualitative network modeling of the MYC-p53 control system of cell proliferation and differentiation. *Biophysical Journal*. 2011; 101(9):2082–2091. <https://doi.org/10.1016/j.bpj.2011.09.052> PMID: 22067145
83. Kobayashi T, Kakizaki I, Nozaka H, Nakamura T. Chondroitin sulfate proteoglycans from salmon nasal cartilage inhibit angiogenesis. *Biochem Biophys Rep*. 2016; 9:72–78. <https://doi.org/10.1016/j.bbrep.2016.11.009> PMID: 28955991
84. Koh I, Cha J, Park J, Choi J, Kang SG, Kim P. The mode and dynamics of glioblastoma cell invasion into a decellularized tissue-derived extracellular matrix-based three-dimensional tumor model. *Sci Rep*. 2018; 8(1):4608. <https://doi.org/10.1038/s41598-018-22681-3> PMID: 29545552
85. Lee S, Han H, Koo H, Na JH, Yoon HY, Lee KE, et al. Extracellular matrix remodeling in vivo for enhancing tumor-targeting efficiency of nanoparticle drug carriers using the pulsed high intensity focused ultrasound. *J Control Release*. 2017; 263:68–78. <https://doi.org/10.1016/j.jconrel.2017.02.035> PMID: 28257990
86. Rape A, Ananthanarayanan B, Kumar S. Engineering strategies to mimic the glioblastoma microenvironment. *Adv Drug Deliv Rev*. 2014; 79–80:172–83. <https://doi.org/10.1016/j.addr.2014.08.012> PMID: 25174308
87. Gotoh N. Regulation of growth factor signaling by FRS2 family docking/scaffold adaptor proteins. *Cancer Sci*. 2008; 99(7):1319–25. <https://doi.org/10.1111/j.1349-7006.2008.00840.x> PMID: 18452557
88. Kim J, Kim PH, Kim SW, Yun CO. Enhancing the therapeutic efficacy of adenovirus in combination with biomaterials. *Biomaterials*. 2012; 33(6):1838–50. <https://doi.org/10.1016/j.biomaterials.2011.11.020> PMID: 22142769
89. Black PC, Agarwal PK, Dinney CP. Targeted therapies in bladder cancer—an update. *Urol Oncol*. 2007; 25(5):433–8. <https://doi.org/10.1016/j.urolonc.2007.05.011> PMID: 17826665
90. Morrison J, Briggs SS, Green N, Fisher K, Subr V, Ulbrich K, et al. Virotherapy of ovarian cancer with polymer-cloaked adenovirus retargeted to the epidermal growth factor receptor. *Mol Ther*. 2008; 16(2):244–51. <https://doi.org/10.1038/sj.mt.6300363> PMID: 18071336
91. Green NK, Morrison J, Hale S, Briggs SS, Stevenson M, Subr V, et al. Retargeting polymer-coated adenovirus to the FGF receptor allows productive infection and mediates efficacy in a peritoneal model of human ovarian cancer. *J Gene Med*. 2008; 10(3):280–9. <https://doi.org/10.1002/jgm.1121> PMID: 18214996
92. Han J, Alvarez-Breckenridge CA, Wang QE, Yu J. TGF-beta signaling and its targeting for glioma treatment. *Am J Cancer Res*. 2015; 5(3):945–55. PMID: 26045979
93. Coniglio SJ, Eugenin E, Dobrenis K, Stanley ER, West BL, Symons MH, et al. Microglial stimulation of glioblastoma invasion involves epidermal growth factor receptor (EGFR) and colony stimulating factor 1 receptor (CSF-1R) signaling. *Molecular medicine*. 2012; 18(3):519. <https://doi.org/10.2119/molmed.2011.00217> PMID: 22294205
94. Pyonteck SM, Akkari L, Schuhmacher AJ, Bowman RL, Sevenich L, Quail DF, et al. CSF-1R inhibition alters macrophage polarization and blocks glioma progression. *Nat Med*. 2013; 19(10):1264–72. <https://doi.org/10.1038/nm.3337> PMID: 24056773
95. Verheije MH, Lamfers ML, Wurdinger T, Grinwis GC, Gerritsen WR, van Beusechem VW, et al. Coronavirus genetically redirected to the epidermal growth factor receptor exhibits effective antitumor

- activity against a malignant glioblastoma. *J Virol.* 2009; 83(15):7507–16. <https://doi.org/10.1128/JVI.00495-09> PMID: 19439466
96. Duzgun Z, Eroglu Z, Avci CB. Role of mTOR in glioblastoma. *Gene.* 2016; 575(2 Pt 1):187–90. <https://doi.org/10.1016/j.gene.2015.08.060> PMID: 26341051
 97. Grogan PT, Sarkaria JN, Timmermann BN, Cohen MS. Oxidative cytotoxic agent withaferin A resensitizes temozolomide-resistant glioblastomas via MGMT depletion and induces apoptosis through Akt/mTOR pathway inhibitory modulation. *Invest New Drugs.* 2014; 32(4):604–17. <https://doi.org/10.1007/s10637-014-0084-7> PMID: 24718901
 98. Liao EC, Hsu YT, Chuah QY, Lee YJ, Hu JY, Huang TC, et al. Radiation induces senescence and a bystander effect through metabolic alterations. *Cell Death Dis.* 2014; 5:e1255. <https://doi.org/10.1038/cddis.2014.220> PMID: 24853433
 99. Kettenmann H, Hanisch U, Noda M, Verkhratsky A. Physiology of microglia. *Physiol Rev.* 2011; 91(2):461–553. <https://doi.org/10.1152/physrev.00011.2010> PMID: 21527731
 100. Wei J, Gabrusiewicz K, Heimberger A. The controversial role of microglia in malignant gliomas. *Clin Dev Immunol.* 2013; 2013:285246. <https://doi.org/10.1155/2013/285246> PMID: 23983766
 101. Markovic DS, Vinnakota K, Chirasani S, Synowitz M, Raguet H, Stock K, et al. Gliomas induce and exploit microglial MT1-MMP expression for tumor expansion. *Proc Natl Acad Sci USA.* 2009; 106:12530–12535. <https://doi.org/10.1073/pnas.0804273106> PMID: 19617536
 102. Crespo S, Kind M, Arcaro A. The role of the PI3K/AKT/mTOR pathway in brain tumor metastasis. *J Cancer Metastasis Treat.* 2016; 2:80–9. <https://doi.org/10.20517/2394-4722.2015.72>
 103. Sampaio NG, Yu W, Cox D, Wyckoff J, Condeelis J, Stanley ER, et al. Phosphorylation of CSF-1R Y721 mediates its association with PI3K to regulate macrophage motility and enhancement of tumor cell invasion. *J Cell Sci.* 2011; 124:2021–31. <https://doi.org/10.1242/jcs.075309> PMID: 21610095
 104. Yoo JY, Hurwitz BS, Bolyard C, Yu J, Zhang J, Selvendiran K, et al. Bortezomib-Induced Unfolded Protein Response Increases Oncolytic HSV-1 Replication Resulting in Synergistic Antitumor Effects. *Clin Cancer Res.* 2014; 20(14):3787–3798. <https://doi.org/10.1158/1078-0432.CCR-14-0553> PMID: 24815720
 105. Yoo JY, Jaime-Ramirez AC, Bolyard C, Dai H, Nallanagulagari T, Wojton J, et al. Bortezomib treatment sensitizes oncolytic HSV-1 treated tumors to NK cell immunotherapy. *Clin Cancer Res.* 2016; pii: clincanres.:1003.2016. <https://doi.org/10.1158/1078-0432.CCR-16-1003>
 106. Kim Y, Lee HG, Dmitrieva N, Kim J, Kaur B, Friedman A. Chondroitinase ABC I-mediated enhancement of oncolytic virus spread and anti-tumor efficacy: A mathematical model. *PLoS One.* 2014; 9(7): e102499. <https://doi.org/10.1371/journal.pone.0102499> PMID: 25047810
 107. Silver DJ, Siebzehnrubl FA, Schildts MJ, Yachnis AT, Smith GM, Smith AA, et al. Chondroitin sulfate proteoglycans potently inhibit invasion and serve as a central organizer of the brain tumor microenvironment. *The Journal of Neuroscience.* 2013; 33(39):15603–15617. <https://doi.org/10.1523/JNEUROSCI.3004-12.2013> PMID: 24068827
 108. Silver DJ, Silver J. Contributions of chondroitin sulfate proteoglycans to neurodevelopment, injury, and cancer. *Curr Opin Neurobiol.* 2014; 27:171–8. <https://doi.org/10.1016/j.conb.2014.03.016> PMID: 24762654
 109. Kundu S, Forsberg-Nilsson K. Glycosaminoglycans and Glioma Invasion. *Eur Assoc NeuroOncol Mag.* 2014; 4(2):75–80.
 110. Kim Y, Stolarska M, Othmer HG. A hybrid model for tumor spheroid growth in vitro I: Theoretical development and early results. *Math Models Methods in Appl Scis.* 2007; 17:1773–1798. <https://doi.org/10.1142/S0218202507002479>
 111. Stolarska M, Kim Y, Othmer HG. Multiscale Models of Cell and Tissue Dynamics. *Phil Trans Roy Soc A.* 2009; 367:3525–3553. <https://doi.org/10.1098/rsta.2009.0095>
 112. Kim Y, Stolarska M, Othmer HG. The role of the microenvironment in tumor growth and invasion. *Prog Biophys Mol Biol.* 2011; 106:353–379. <https://doi.org/10.1016/j.pbiomolbio.2011.06.006> PMID: 21736894